AD_____

Award Number: W81XWH-06-01-0791

TITLE: Development and Optimization of a Dedicated, Hybrid Dual-Modality SPECT–CmT System for Improved Breast Lesion Diagnosis

PRINCIPAL INVESTIGATOR: Priti Madhav

CONTRACTING ORGANIZATION: Duke University
Durham NC 27708

REPORT DATE: January 2009

TYPE OF REPORT: Annual Summary

PREPARED FOR: U.S. Army Medical Research and Materiel Command
Fort Detrick, Maryland 21702-5012

REPORT DOCUMENTATION PAGE

Form Approved
OMB No. 0704-0188

1. REPORT DATE	2. REPORT TYPE	3. DATES COVERED
1 Jan 2009	Annual Summary	1 Jan 2008 – 31 Dec 2008

4. TITLE AND SUBTITLE

Development and Optimization of a Dedicated, Hybrid Dual-Modality SPECT–CmT System for Improved Breast Lesion Diagnosis

5a. CONTRACT NUMBER

5b. GRANT NUMBER
W81XWH-06-01-0791

5c. PROGRAM ELEMENT NUMBER

6. AUTHOR(S)

Priti Madhav

E-Mail: priti.madhav@duke.edu

5d. PROJECT NUMBER

5e. TASK NUMBER

5f. WORK UNIT NUMBER

7. PERFORMING ORGANIZATION NAME(S) AND ADDRESS(ES)

Duke University
Durham NC, 27708

8. PERFORMING ORGANIZATION REPORT NUMBER

9. SPONSORING / MONITORING AGENCY NAME(S) AND ADDRESS(ES)
U.S. Army Medical Research and Materiel Command
Fort Detrick, Maryland 21702-5012

10. SPONSOR/MONITOR'S ACRONYM(S)

11. SPONSOR/MONITOR'S REPORT NUMBER(S)

12. DISTRIBUTION / AVAILABILITY STATEMENT
Approved for Public Release; Distribution Unlimited

13. SUPPLEMENTARY NOTES

14. ABSTRACT

The overall objective of this project is to implement a dual-modality single photon emission computed tomography (SPECT) and x-ray computed mammotomography (CmT) system for the detection and staging of breast cancer, monitoring of treatment therapies, and improving surgical biopsy guidance. The sequential acquisition with emission (nuclear) and transmission (x-ray) 3D imaging systems can aid in localizing the radioactive uptake of a tumor from the emission image by using the anatomical structure from the transmission image. In the second year, CmT artifacts due to the lateral offset geometry and scatter were investigated. Using the data acquisition sequence developed in Year 1, a couple of patient studies were also completed to demonstrate the strength in 3D volumetric dual-modality imaging with the dedicated SPECT-CmT breast scanner. Other aspects of the training program have been initiated including acceptance of one manuscript to a peer-reviewed journal and presentations at various local and international conferences.

15. SUBJECT TERMS
X-ray imaging, Nuclear Medicine Imaging, SPECT, CT, Molecular Breast Imaging, Mammotomography

16. SECURITY CLASSIFICATION OF:			17. LIMITATION OF ABSTRACT	18. NUMBER OF PAGES	19a. NAME OF RESPONSIBLE PERSON
a. REPORT	b. ABSTRACT	c. THIS PAGE			USAMRMC
U	U	U	UU	29	19b. TELEPHONE NUMBER *(include area code)*

Table of Contents

A. INTRODUCTION

The overall objective of this project is to implement a dual-modality single photon emission computed tomography (SPECT) and x-ray computed mammotomography (CmT) system for the detection and staging of breast cancer, monitoring of treatment therapies, and improving surgical biopsy guidance. The sequential acquisition with emission (nuclear) and transmission (x-ray) 3D imaging systems can aid in localizing the radioactive uptake of a tumor from the emission image by using the anatomical structure from the transmission image. In the second year, CmT artifacts due to the lateral offset geometry and scatter were investigated. Using the data acquisition sequence developed in Year 1, a couple of patient studies were also completed to demonstrate the strength in 3D volumetric dual-modality imaging with the dedicated SPECT-CmT breast scanner. Other aspects of the training program have been initiated including acceptance of one manuscript to a peer-reviewed journal and presentations at various local and international conferences.

B. BODY

The Statement of Works along with the original projected timeline is attached in Appendix A of this Progress Report. In Year 1, Task 1 was completed including a couple of parts that had been initially proposed to be finished in Year 2. In addition, Task 3(a), which was originally proposed to be fulfilled in Year 2, was also carried out in Year 1. In the following sections, a modified timeline has been added to each listed task to indicate the time spent on each project in Year 2. As a reference, Figure 1 illustrates a 3D CAD depiction of the current dedicated dual-modality SPECT-CmT scanner with a customized patient bed.

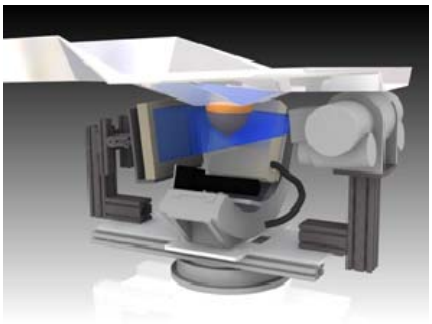

FIGURE 1: 3D CAD image of SPECT-CmT dedicated breast scanner with a customized patient bed and a breast (orange) in the FOV. The CmT cone-beam source is shown in blue.

Task 2: Optimize CmT system by applying corrections to improve image quality

Task 2(a): Reduction of Circular Artifacts in Reconstructions due to Lateral Offset Geometry (Months 13-16)

Artifacts have shown to degrade the quality of CmT images. To optimize the image quality, it is necessary to understand the cause of these artifacts and find out how to avoid and suppress them. In the beginning of Year 2, the first artifact that was investigated was the circular artifact seen in the CmT reconstructed coronal slices (or cylinder in sagittal slices) acquired with a lateral offset geometry (Fig. 2). In this geometry, the CmT system is placed 5cm offset from the rotational axis. The advantage of such an arrangement is that objects larger than the field-of-view (FOV) of the detector can be scanned without being truncated. Studies have shown that circular artifacts in CmT images can be caused by nonuniformity effects among detector elements, misaligned geometry, etc. [1, 2]. If the cause was detector nonuniformity, ring (or cylinder) artifacts would have also been seen in the images acquired with a centered geometry (Fig. 2). Therefore, a study was done to see if mechanical misalignments would lead to similar type artifacts in the reconstructed images. To do this, Monte Carlo simulations using PENELOPE was performed by creating an object similar to the Defrise phantom (Fig. 3) and setting the detector at different tilts. The CmT system was configured in Monte Carlo to complement the setup of the built prototype. The x-rays was set as a 28° cone-beam source with energy spectra matching the actual CmT source [3]. The material used for the detector was cesium-iodide (CsI) with dimensions of 17.9x23.8cm. Source-to-image distance (SID) and source-to-object distance (SOD) was 60cm and 38.18cm, respectively. The size of each projection

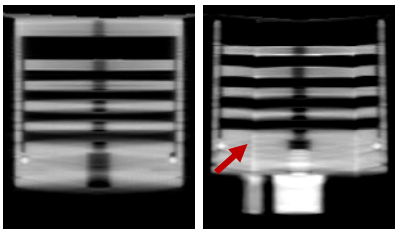

FIGURE 2: CmT reconstructed sagittal slices of the Defrise phantom acquired with (left) centered and (right) offset geometry. Due to the offset geometry, the image has a cylindrical artifact (shown by the red arrow) along with slight distortion in the discs and outer case.

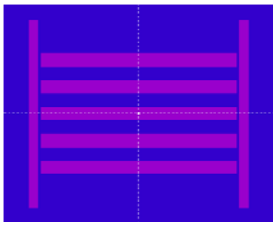

FIGURE 3: Side profile of the Defrise phantom drawn in PENELOPE. Outer and inner cylinder is 8.2cm and 7.5cm in diameter, respectively. Each of the 5 discs (in between the cylinder) is 0.25cm thick and 7.3cm diameter. The spacing between each disc is 1cm.

image was 144x192pixels with each pixel being 0.1240cm. Final projection images were iteratively reconstructed using an ordered subsets transmission algorithm. Reconstruction parameters was set to 5 iterations, 8 subsets, 350x350x384 reconstruction grid and 0.1240cm^3 voxel size.

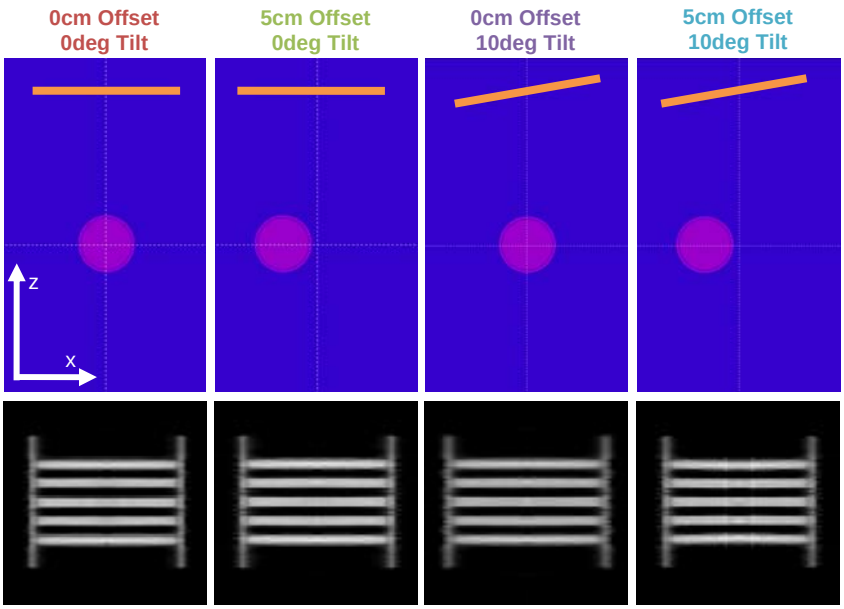

FIGURE 4: (top) Top down view of the four different setups with the phantom (purple circle) and CmT detector (orange line). Axis is shown with the y-axis coming up from the page. Intersection of the dotted lines represents the location of the system's rotational axis. (bottom) CmT reconstructed sagittal slice of each setup shown accordingly.

Figure 4 shows the four different CmT setups: (1) phantom at the center-of-rotation (COR) and no detector misalignment; (2) phantom 5cm offset from the COR and no detector misalignment; (3) phantom at the COR and detector tilted 10° respect to the y-axis; and (4) phantom 5cm offset from the COR and detector tilted 10° respect to the y-axis. Final reconstructed images showed that in an ideal situation with no detector tilt, there was no visible cylindrical artifact irrespective of offset. However with a detector tilt, a cylindrical artifact was only seen in the offset geometry. This was similar to what was seen with the actual reconstructed images collected with a Defrise phantom on the built system (Fig. 2). A line profile taken through the center of the middle (3rd from top) disc confirms the cylindrical artifact seen in the 5cm offset and 10° tilt case with the sudden noticeable spike in pixel value (Fig. 5). It should be noted that the reason pixel values through the disc for all four setups are not consistent with each other is due to the random sampling of Monte Carlo simulations which can produce thousands of outcomes (in contrast to discrete results),

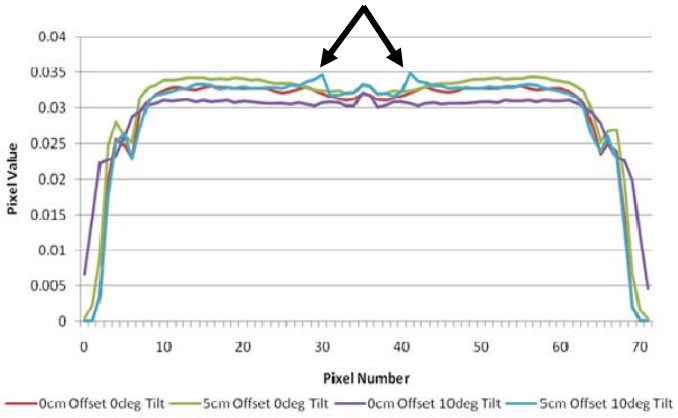

FIGURE 5: Line profile taken through the center of the middle disc of the Defrise phantom for each CmT reconstructed slice in Fig. 4. Black arrows point to this spike in pixel value due to the circular artifact in the offset geometry case with the tilted detector.

To get an accurate position of the detector, a machine tool called Microscribe 3D-MX (*Immersion Corporation*, San Jose, CA) was additionally used to find the position of the detector relative to the base plate, which lies on top of the rotation stage and secures both imaging systems. To do this, a point on the base plate was calibrated as being the center point. Relative to this center point, four points were collected on all four corners of the detector. Results showed that the detector was ~7.5°, ~1.8°, ~1.3° tilted respect to x-, y-, and z-axis, respectively. Ideally the detector should be 6.2°, 0°, 0° tilted respect to x-, y-, and z-axis, respectively. However, it was mechanically difficult to place the detector in this position.

In conclusion, these Monte Carlo studies illustrated that an offset geometry with a slight detector tilt can yield a circular ring and cylindrical artifact in the coronal and sagittal reconstructed slices, respectively. However, this artifact can be effectively eliminated by placing the system in a centered geometry regardless of detector tilt. Therefore, the entire CmT system has currently been shifted to a centered geometry. Based on MRI images, a study found that an average breast size is 8.2cm for nipple-to-chest wall, 10.5cm for superior-inferior, and 14.1cm medial-lateral [4]. These measurements assured that the image of an average breast would not be truncated with our current 20x25cm detector and therefore going with a centered geometry would not be an issue.

Task 2(b): CmT Scatter Correction (Months 20-24)

This work was originally proposed to begin in Year 3, but due to the understood complexity of the project it was started earlier. The second artifact addressed was the physical effects, specifically scatter, which can degrade image quality. In studies pertaining to cone-beam CmT systems, few groups have found scatter to be an important factor in image quality degradation [5-8]. Scattered photons, which have been deflected from its original direction, reduce the photon beam intensity resulting in image blur and degradation. The magnitude and effect that scatter can have on an image primarily depends on the imaging system and geometry, acquisition parameters, and object size and composition. There have been several investigations in pre-acquisition scatter control techniques including use of an anti-scatter grid [9, 10], air gap (increase in SID) [11], and reduction of field size. However in this study, I investigated a post-acquisition scatter correction technique to estimate the scatter distribution in each projection image. In this method, a beam stop array (BSA), which consists of a regularly spaced array of radio-opaque absorbers, is placed directly in front of the x-ray beam to absorb all the primary radiation. Consequently, the final projection image will have an array of shadowed areas. Since it is assumed that all the primary x-ray photons are blocked by the radio-opaque absorbers, any radiation detected within each shadowed area is presumed to be entirely due to scatter.

The first step was to create a BSA to place in front of the collimator of the x-ray tube. After investigating different shapes (i.e. spheres, circular disks) and materials (i.e. lead, tungsten carbide) to use for the radio-opaque absorbers, lead spheres was chosen. Spheres were chosen over circular disks due to the divergent angle of the x-rays that travel away from the central ray of the cone-beam. Unlike the disks, the path length of the x-rays penetrating through the center of the sphere will be the same irrespective of the angle in which the rays arrive. As a result, the spheres retain its shape throughout the image while the disks appear more elliptical toward the edges of the image. With a higher attenuation coefficient, lead is also more favorable than tungsten carbide in blocking primary x-rays.

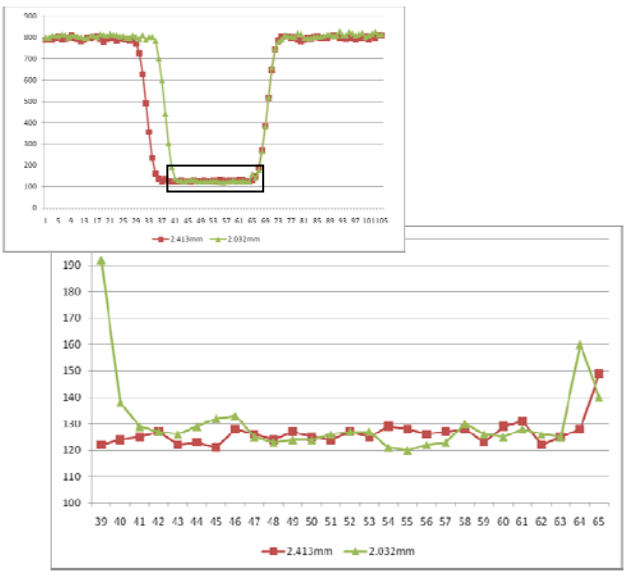

FIGURE 6 (top) Line profile across a single lead shot with diameters of 2.032 and 2.413mm. (bottom) Enlarged view of the profile marked by the black box.

The next step was determining the optimal sphere diameter. Choosing a large enough size was essential to stop all the incident primary radiation but small enough to permit as many possible scatter measurements throughout the image. Lead shots with diameters ranging from 2.032mm to 3.048mm (*McMaster-Carr*, Atlanta, GA) were purchased and investigated. Single-shot projection images were acquired for each lead bead taped to the front of the collimator. A line profile taken through each bead did not show a significant difference (Fig. 6), and thus, the smallest, 2.032mm, diameter lead sphere was chosen. According to Beer's Law, the amount of transmittance through the lead bead is 1.7×10^{-21}, which is negligible. Contrary to this calculation, the plot in Figure 6 (bottom) reveals some x-ray photons being detected behind the lead sphere. This could likely be due to a DC offset in the detector.

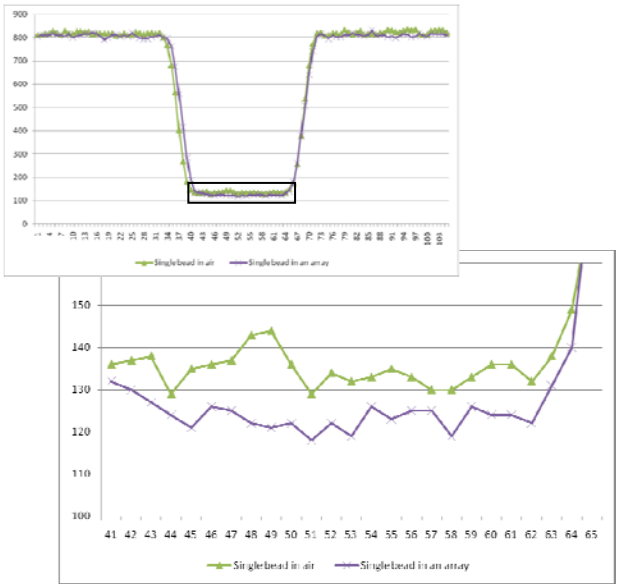

FIGURE 7 (top) Line profile across a single lead bead in air and in an array with multiple beads. (bottom) Enlarged view of the profile marked by the black box.

Another effect to consider was the crosstalk between the lead spheres. This was examined by acquiring single-shot projection images of a single bead and a regularly spaced array of beads and comparing

line profiles taken through the center of a single lead sphere. Figure 7 shows that the pixel values of the bead in an array were slightly lower than a single bead. The cause of this scatter reduction in an array of beads may be due to a decrease in the amount of primary radiation in the FOV that can scatter since more x-rays are blocked with the lead shots. If this reduction will make an impact on the final measurements, it will have to be taken into account when calculated the scatter image.

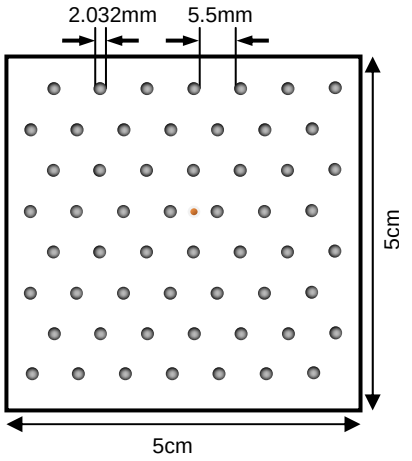

FIGURE 8: Illustration of the BSA with lead beads (gray circles) arranged in a hexagonal array. Dimensions are shown.

Finally, it was decided to position the lead spheres in a hexagonal array rather than the conventional square arrangement (Fig. 8). This layout was preferred since more beads can be positioned and in turn attain more discrete scatter measurements. In Year 3, this array of ball bearings will be embedded into holes drilled in a 5x5cm acrylic plate and attached to the end of the collimator box which is about 15cm away from the x-ray focal spot. Each bead will be spaced 7.032mm apart so its shadow in the image is approximately 22mm apart. The shadows have to be kept a good distance apart such that any scatter measurements made within each region will exclusively be due to scatter in that area and not be affected by the surrounding beads.

Concurrently with creating a BSA, a scatter algorithm has been partly written in MATLAB. The sequence of the algorithm is as follows:

1. Load a projection with the BSA in the FOV to find the *x*,*y* center position of all the lead spheres in the image. Currently, this is done semi-automatically. The user firsts enters the quantity and diameter of the beads and continues to manually select each center point. Based on the given information and surrounding pixel values, the program proceeds to reposition the user-selected center point such that it is exactly in the middle of the sphere. It is expected that once the BSA has been created, the location of the spheres will be coded into the algorithm and this step might not be necessary.
2. Load another projection with only the object in the FOV. The object is segmented by using a k-means algorithm.
3. Load a third projection with the object and BSA in the FOV. Based on the bead location and segmentation result from the previous steps, scatter is only measured inside the object.
    a. Currently, a single scatter value is measured only at the center point of each sphere. This will later be modified to an average scatter measurement over a small ROI around the center point.
    b. Next, a single scatter value was calculated in the middle of each pair of beads. Figure 8 illustrates one of these locations by an orange circle. As it's seen, this measurement can be either calculated along each row or column of spheres. Therefore, first a 1D cubic spline interpolation (pre-written MATLAB function) was performed along each row and column that intersected the spheres' center points to calculate the scatter value at this location (i.e. orange circle in Fig. 8). The interpolated values were then weighted and summed to give the final scatter value at each of these positions.
    c. Using a 2D cubic spline interpolation (pre-written MATLAB function), scatter was calculated for all points in the image.
4. The scatter image is subtracted from the original image to yield an image with only primary photons.

Figure 9 presents an example of how the beam array might look along with the projection images. These projections were acquired to test and debug the scatter algorithm written in MATLAB.

In Year 3, this algorithm will be extended to measure the scatter for all 240 projections. After taking scatter measurements from a few projections, a 2D interpolation routine (pre-written MATLAB function) will be employed in estimating the scatter for all the remaining projections

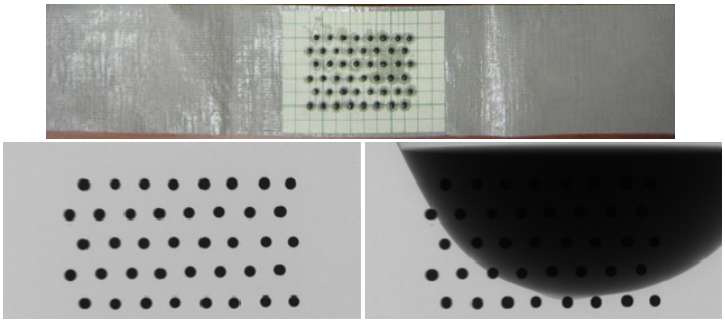
FIGURE 9: (top) BSA with lead beads arranged in a hexagonal array and glued to a grid paper. Each bead is 5mm apart. BSA is attached to duct tape which was then placed in front of x-ray collimator (bottom) CmT projections of grid (left) without object and (right) with water-filled breast phantom.

without the BSA. A study will also be conducted on finding the optimal number and location of projections with a BSA needed to measure as accurately as possible the amount of scatter in all images. In addition, different interpolation routines will be looked at to see if a better estimation of scatter can be obtained. Once the BSA and algorithm is done, this scatter technique can be applied to all CmT acquisitions and tests will be performed to analyze the change in the reconstructed images.

Unlisted Task: Hybrid SPECT-CmT Patient Studies (Months 17-19)

Patient studies using the hybrid SPECT-CmT system was never written in the Statement of Works. Funding from this project came from my advisor's NIH R01 grant and not this DOD pre-doctoral fellowship. It is shown here for illustration purposes and demonstration of the system's clinical potential. During the middle of Year 2, a couple of volunteers with biopsy confirmed breast cancer was scanned on the dual-modality system. The data acquisition sequence that was proposed in Year 1 was employed. All patients were imaged under a protocol approved by the Duke University Medical Center institutional review board (IRB) and informed written consent was obtained. This work was presented at the *2008 Duke Cancer Comprehensive Cancer Center annual meeting*, *2008 DOD BCRP Era of Hope Meeting*, and *2008 AAPM (American Association of Physicists in Medicine) annual conference*. The abstracts are attached in Appendix B-D.

The first patient in Year 2 was only scanned with the CmT system at a -6.2° tilt and offset geometry. Tube potential was set at 60kVp with a 1.25mAs exposure. Along with biopsy confirmed breast cancer, this patient also had a breast implant. In mammography, imaging patients with breast implants can be a difficult task since there is a risk of implant rupture due to compression and obstruction of detecting possible cancer in the tissue due to tissue/implant superposition in the images. Figure 10 displays the acquired reconstructed slices. These images demonstrate the superior ability of fully volumetric imaging to differentiate among glandular and adipose tissue and implants. The cylindrical artifact is due to the offset geometry (further explanation in *Task 2(a)*).

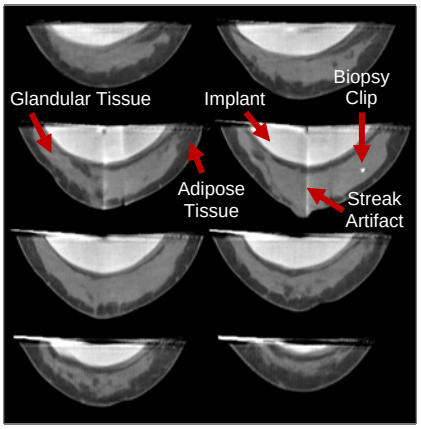

FIGURE 10: CmT reconstructed sagittal slices of a breast cancer patient (42yrs, 68kg) with implant and biopsy clip.

The second patient was scanned with both imaging systems. This patient had a biopsy confirmed DCIS anterior to her chest wall. Prior to the scan, the subject was injected with 660MBq of ^{99m}Tc-sestamibi and had four fiducial markers (i.e. nylon balls) previously soaked in ^{99m}Tc taped at 3, 6, 9, and 12 o'clock position. The CmT scan was first carried out at a -6.2° tilt and centered geometry. Tube potential was set at 60kVp with a 1.25mAs exposure. After this acquisition, SPECT was performed using a 15-45° PROJSINE (three-lobed sinusoid) trajectory which was specifically constructed to contour the patient's breast [12]. Final CmT reconstructed images showed the location of the biopsy clip. However, the SPECT images showed that there were signs of Tc^{99m}-sestamibi uptake underneath the biopsy clip signifying a suspecting lesion in this patient (Figure 11). This was confirmed in MRI images. This hybrid study illustrates the significance of using functional information from SPECT to localize the lesion in the anatomical CmT images.

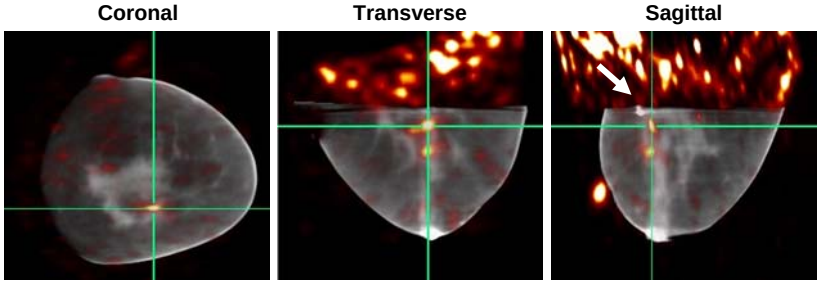

FIGURE 11: Fused SPECT-CmT reconstructed slices of a breast cancer patient (54yrs, 96kg). Green hashmarks indicate radiotracer uptake by the suspected lesion. Above this area is a previously placed biopsy clip (shown by the white arrow). Bright areas above breast are radiotracer uptake by heart and liver.

The CmT system uses a quasi-monochromatic x-ray source [13] which can improve the visualization of tissues with very small differences in attenuation coefficients along with using a low x-ray dose. Additionally, we have shown elsewhere that this beam eliminates the well known CT beam hardening artifact, and that global changes across the field of an object are due mainly to scatter and sampling. This is crucial since the difference between attenuation coefficients of normal and cancerous lesion especially at lower energies is minimal [14]. The benefit of using a quasi-monochromatic source is shown with an image histogram taken from

a subject scanned in 2007 (Fig. 12). Based on attenuation coefficients, this histogram shows a clear distinction among the different tissues and suspected cancerous lesion. Broadening of the peaks is presumed to be caused by the lack of scatter compensation in the images. However, once scatter is accounted for, these peaks are expected to be narrower in conjunction with a more uniform attenuation value for each tissue.

It is expected that there will be more patient scans in Year 3.

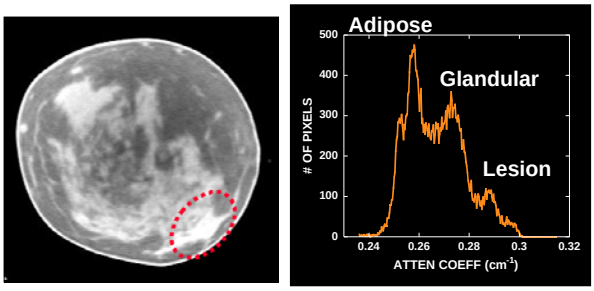

FIGURE 12: (left) CmT reconstructed coronal slice of biopsy confirmed breast cancer patient (45yrs, 93kg). Red dotted circle shows location of suspected lesion. (right) Image histogram of this slice. Each peak is labeled respectively.

Task 4: Complete other aspects of the breast cancer training program

Task 4(b): Publish work in journals (Months 15-24)

Three manuscripts have been worked on for submission to peer-reviewed journals during the majority of Year 2. One paper on the modular transfer function (MTF) measurements made with 3D SPECT has successfully been accepted to the *IEEE Transactions of Nuclear Science* (attached in Appendix E) and its expected date of publication is June 2009. Other papers that are still in the works are MTF measurements with 3D CmT (expected publication in *Medical Physics*) and effect of cone-beam tilted CmT source on distortion and artifacts in images (expected publication in *Physics of Medicine and Biology*).

Task 4(c): Attend and present at local conferences (Month 15)

As mentioned in the *Unlisted Task*, hybrid patient studies were presented at the *2008 Duke Cancer Comprehensive Cancer Center annual meeting* in March 2008. Abstract is attached in Appendix B.

Task 4(d): Attend and present at interntional conferences (Months 18-19, 22-23)

Implementation of the dedicated breast SPECT-CmT imaging system and patient studies were presented at the *2008 DOD BCRP Era of Hope Meeting* and *2008 AAPM annual meeting* (abstracts attached in Appendix C-D). The *2008 IEEE Medical Imaging Conference*, *2008 Molecular Breast Cancer Workshop*, and *2008 Radiological Society of North America (RSNA) annual meeting* were attended. Although none of my research work was presented here, it was great to see the clinical aspects of medical imaging and learn more about other modalities involved in breast cancer detection.

C. KEY RESEARCH ACCOMPLISHMENTS

From the original proposed Statement of Works, Year 2 included Tasks 1(d), Task 2(a), Task 3(a) and 4(b-d) (Appendix A). Since Task 1(d) and Task 3(a) had already been completed in Year 1, this was not showed in the current progress report. Elements of Task 2(b) have also been in development although it was promised in Year 3.

- Investigated cause of circular (or cylindrical) artifact in offset images proposed in Task 2(a). Simulations found that the cause was due to a detector misalignment in the offset geometry and could be eliminated by setting the system in a centered geometry despite the slight tilt in the detector.
- Proposed a beam stop array to use to measure scatter and wrote majority of code to implement scatter correction. Although this task (Task 2(b)) was proposed in Year 3, preliminary work has already started and will be completed in the coming months.
- Performed scans on several subjects to show the benefit of 3D volumetric fused imaging, use of quasi-monochromatic source, and no breast compression. This work was presented at *2008 Duke Cancer*

Comprehensive Cancer Center annual meeting, *2008 DOD BCRP Era of Hope Meeting*, and *2008 AAPM annual meeting*. Abstracts are attached in Appendix B-D.

- Had manuscript accepted for publication in *IEEE Transactions of Nuclear Science* (Appendix E). Expected publication date is in June 2009.
- Contributed work to three additional presentations presented at the *2008 IEEE Medical Imaging Conference* and *2008 Molecular Breast Cancer Workshop* (Appendix F-H).

Related

- Won a Young Investigator Award for presentation at the *2008 Duke Cancer Comprehensive Cancer Center Annual Meeting*.
- Interviewed by few news media outlets regarding work on patient SPECT-CmT studies presented at the *2008 AAPM Annual Meeting* (see below).
- Received a Masters in Biomedical Engineering based on courses and research.

D. REPORTABLE OUTCOMES

Peer-Reviewed Papers

P Madhav, JE Bowsher, CN Brzymialkiewicz, SJ Cutler, MP Tornai. "Characterizing the MTF in 3D for a quantized SPECT camera having arbitrary trajectories." Accepted to *IEEE Trans Nucl Sci.*

Conference Proceedings

SJ Cutler, KL Perez, **P Madhav**, MP Tornai. "Comparison of 2D scintimammography and 3D dedicated breast SPECT using a compressible breast phantom and lesions of varying size and tracer uptake." Presented at the *2008 IEEE Fourth International Workshop on the Molecular Radiology of Breast Cancer*, Dresden, Germany, 20-21 Oct. 2008 and published in *IEEE Conference Record NSS/MIC*.

KL Perez, SJ Cutler, **P Madhav**, MP Tornai. "Novel patient acquisition trajectories for optimized dedicated breast SPECT imaging." Presented at the *2008 IEEE Fourth International Workshop on the Molecular Radiology of Breast Cancer*, Dresden, Germany, 20-21 Oct. 2008 and published in *IEEE Conference Record NSS/MIC*.

DJ Crotty, SJ Cutler, RL McKinley, **P Madhav**, KL Perez, MP Tornai. "Improved chest wall imaging through combined complex trajectories in dedicated dual modality SPECT-CT breast molecular imaging." Presented at the *2008 IEEE Fourth International Workshop on the Molecular Radiology of Breast Cancer*, Dresden, Germany, 20-21 Oct. 2008 and published in *IEEE Conference Record NSS/MIC*.

Abstracts and Presentations

DJ Crotty, **P Madhav**, SJ Cutler, KL Perez, RL McKinley, MP Tornai, "Performance of a new dual-modality molecular-anatomical imaging system dedicated to breast cancer." Presented at the *2008 Duke Cancer Center Annual Meeting*, Durham, NC, 10 Mar. 2008.

P Madhav, SJ Cutler, DJ Crotty, KL Perez, RL McKinley, PK Marcom, TZ Wong, MP Tornai. "Dedicated molecular and anatomical breast imaging - initial patient studies." Presented at the *2008 Duke Cancer Center Annual Meeting*, Durham, NC, 10 Mar. 2008.

P Madhav, MP Tornai. "Development and optimization of a dedicated, hybrid dual-modality SPECT-CmT system for improved breast lesion diagnosis." Presented at the *2008 Era of Hope Conference*, Baltimore, MD, 25-28 Jun 2008.

P Madhav, SJ Cutler, DJ Crotty, KL Perez, RL McKinley, L Wilke, TZ Wong, MP Tornai. “Pilot patient studies using a dedicated dual-modality SPECT-CT system for breast imaging.” Presented at the *2008 American Association of Physicists in Medicine Meeting*, Houston, TX, 27-31 Jul. 2008, and published in Med. Phys. 35(6): 2894.

Media

Schirber, Michael. “News Release: Cancer Research Highlights: Hybrid imager could improve breast exams.” [Online document] July 2008. Available at HTTP: http://www.aapm.org/meetings/08AM/VirtualPressRoom/HighlightedPapers/cancernothree.asp

Stone, Kathyln. “SPECT/CT mammography system produces first patient images.” [Online document] July 2008. Available at HTTP: http://www.auntminnie.com/index.asp?Sec=sup&Sub=mol&Pag=dis&ItemId=81963

Chustecka, Zosia. “Dedicated breast CT scanners more comfortable than mammography.” [Online document] August 2009. Available at HTTP: http://www.medscape.com/viewarticle/578981

E. CONCLUSION

Significant progress has been made in Year 2. CmT artifacts due to lateral offset geometry and scatter have been investigated. The cause of the artifact was shown to be due to a combination of an offset geometry and detector misalignment. Regardless of the detector tilt, centering the system eliminated the artifact. Implementing the scatter algorithm has been initiated with great achievement and should be finished by the end of Year 3. Patient studies (funded by my advisor’s NIH R01 grant) on the dedicated breast hybrid scanner successfully display superior image quality and show the benefit of fused information. A manuscript on 3D MTF measurements in SPECT has successfully been accepted to a peer-reviewed journal and more papers are in the works.

F. REFERENCES

[1] J. F. Barrett and N. Keat, "Artifacts in CT: Recognition and Avoidance," *Radiographics,* vol. 24, pp. 1679-1691, November 1, 2004 2004.

[2] Y. Sun, Y. Hou, and J. Hu, "Reduction of artifacts induced by misaligned geometry in cone-beam CT," *IEEE Trans Biomed Eng,* vol. 54, pp. 1461-71, Aug 2007.

[3] D. J. Crotty, R. L. McKinley, and M. P. Tornai, "Experimental spectral measurements of heavy K-edge filtered beams for x-ray computed mammotomography," *Phys Med Biol,* vol. 52, pp. 603-616, 2007.

[4] S. J. Cutler, D. J. Crotty, and M. P. Tornai, "Dyanmic laser-guided contouring for dedicated emission mammotomography," in *Nuclear Science Symposium Conference Record, 2008. NSS '08. IEEE*, 2008, pp. 4789-4793.

[5] P. M. Joseph and R. D. Spital, "The effects of scatter in x-ray computed tomography," *Med Phys,* vol. 9, pp. 464-472, 1982.

[6] J. H. Siewerdsen and D. A. Jaffray, "Cone-beam computed tomography with a flat-panel image: magnitude and effects of x-ray scatter," *Med Phys,* vol. 28, pp. 220-231, 2001.

[7] A. Malusek, M. Sandborg, and G. Carlsson, "Simulation of scatter in cone beam CT - effects on projection image quality," *2003 SPIE Med Imag Conf,* vol. 5030, pp. 740-751, 2003.

[8] M. Endo, S. Mori, T. Tsunoo, and H. Miyazaki, "Magnitude and effects of x-ray scatter in a 256-slice CT scanner," *Med Phys,* vol. 33, pp. 3359-68, Sep 2006.

[9] J. H. Siewerdsen, D. J. Moseley, B. Bakhtiar, S. Richard, and D. A. Jaffray, "The influence of antiscatter grids on soft-tissue detectability in cone-beam computed tomography with flat-panel detectors," *Med Phys,* vol. 31, pp. 3506-3520, 2004.

[10] J. Wiegert, M. Bertram, D. Schafer, N. Conrads, J. Timmer, and T. A. G. Rose, "Performance of standard fluoroscopy anti-scatter grids in flat detector based cone beam CT," in *2004 SPIE Medical Imaging Conference*, San Diego, CA, 2004, pp. 67-78.

[11] A. L. C. Kwan, J. M. Boone, and N. Shah, "Evaluation of x-ray scatter properties in a dedicated cone-beam breast CT scanner," *Med. Phys.,* vol. 32, pp. 2967-2975, 2005.
[12] C. N. Archer, M. P. Tornai, J. E. Bowsher, S. D. Metzler, B. C. Pieper, and R. J. Jaszczak, "Implementation and initial characterization of acquisition orbits with a dedicated emission mammotomograph," *IEEE Trans. Nucl. Sci.,* vol. 50, pp. 413-420, 2003.
[13] R. L. McKinley, M. P. Tornai, E. Samei, and M. L. Bradshaw, "Initial study of quasi-monochromatic beam performance for x-ray computed mammotomography," *IEEE MIC,* vol. 4, pp. 2999-3003, 2003.
[14] P. C. Johns and M. J. Yaffe, "X-ray characterization of normal and neoplastic breast tissues," *Phys. Med. Biol.,* vol. **32**, pp. 675-695, 1987.

APPENDIX A: STATEMENT OF WORK

Task 1 Design and implement a dual-modality prototype system (Months 1-17):

a. Investigate effect of physical constraints (such as having the SPECT camera partially in front of the x-ray detector) on scatter contamination in reconstructed images. (Months 1-5)
b. Develop software to synchronize both systems during image acquisition. (Months 6-11)
c. Develop an ideal sequence (based on complete sampling, physical constraints) for emission and transmission data acquisition. (Months 11-12)
d. Explore 3D complex orbits with physically possible optimal orientations and tilt angles that can be used to have the system fit underneath the patient bed and still be able to image close to the chest wall. (Months 13-17)

Task 2 Optimize CmT system by applying corrections to improve image quality (Months 18-29):

a. Investigate methods to reduce circular artifacts in reconstruction from CmT images collected with a centered object and laterally offset central x-ray beam. (Months 18-22)
b. Investigate and implement scatter correction methods to CmT images. (Months 23-29)

Task 3 Evaluate SPECT system for quantification measurements of lesion activity (Months 22-36):

a. Perform image registration of SPECT and CmT images using existing image registration algorithm (i.e. surface fitting technique) with the aid of fiducial markers. (Months 22-23)
b. Investigate, implement, and compare two attenuation correction methods (i.e. uniform attenuation distribution, CmT-based attenuation distribution) to apply to SPECT data. (Months 24-30)
c. Perform SPECT quantification measurements incorporating all corrections using phantoms and lesions with known concentration activity. (Months 30-36)

Task 4 Complete other aspects of the breast cancer training program (Months 1-36):

a. Shadow a radiologist(s) to observe the clinical and diagnostic side in breast cancer imaging (Nuclear Medicine, Mammography). (Months 1-12)
b. Publish research work in peer-reviewed journals. (Months 1-36)
c. Attend and present at local seminars offered at Duke University through Medical Physics and the Breast and Ovarian Oncology Research Program, which is part of the Duke Comprehensive Cancer Center. (Months 13-36)
d. Attend international conferences such as SPIE Medical Imaging Conference, DOD BCRP Era of Hope Meeting, IEEE Medical Imaging Conference, RSNA Conference, and San Antonio Breast Cancer Symposium. (Months 13-36)
e. Prepare thesis and defend. (Months 30-36)

APPENDIX B: DUKE COMPREHENSIVE CANCER CENTER ABSTRACT

Dedicated Molecular and Anatomical Breast Imaging - Initial Patient Studies

Priti Madhav, Spencer Cutler, Dominic Crotty, Kristy Perez, Randolph McKinley, Kelly Marcom, Terence Wong, Martin Tornai

Breast cancer is the most commonly diagnosed cancer among women worldwide and is the second leading cause of cancer death in the US. With the limitations and discomfort of mammography, alternative imaging techniques to detect and monitor breast cancer early, reduce unnecessary biopsies, and improve patient comfort have been designed. We have developed a compact, dedicated, dual-modality SPECT (single photon emission computed tomography - a molecular imaging approach) and CT (computed tomography - a diagnostic imaging approach) system, which allows for quantitative 3D volumetric functional and anatomical imaging, respectively, of a pendant, uncompressed breast. Fused images can potentially provide more valuable clinical information for evaluation of cancerous diseases than the independent systems alone. A preliminary investigation on the clinical performance of the hybrid system was done by imaging women with biopsy confirmed breast cancer. With no breast compression and an open, common field-of-view geometry system, the patient lies prone on a customized patient bed while the hybrid device non-invasively acquires 3D data underneath. Using the flexible positioning capability of the gantry, the SPECT subsystem acquires data using a 3D complex trajectory, which permits the camera to get closer to the breast and chest wall. CT images were collected with the system rotating circularly around the breast. Initial human subject studies demonstrated that SPECT images can clearly visualize the tracer uptake by the tumor, and the subsystem has the capability to view into the chest wall. Physical system constraints limited visualization of the chest wall in the CT images. With the elimination of overlapping tissues through 3D imaging, CT images can potentially improve lesion isolation versus conventional screening modalities. Future studies include improved patient positioning for better CT chest inclusion as well as clinical comparisons with mammograms and/or MRI images for quantification of potential improved detection.

Presented at the
2008 Duke Comprehensive Cancer Center Meeting
Durham, NC
10 March, 2008

APPENDIX C: DOD BCRP ERA OF HOPE ABSTRACT

DEVELOPMENT AND OPTIMIZATION OF A DEDICATED, HYBRID DUAL-MODALITY SPECT-CMT SYSTEM FOR IMPROVED BREAST LESION DIAGNOSIS

Priti Madhav and Martin Tornai
Department of Radiology and Biomedical Engineering, Duke University Medical Center, Durham NC;
Email: priti.madhav@duke.edu

Background and Objectives

Independently developed SPECT (single photon emission computed tomography) and CmT (computed mammotomography) subsystems are integrated onto a single gantry to allow 3D volumetric functional/anatomical imaging of a pendant, uncompressed breast in the common field-of-view of both systems (Fig. 1). Fused images can potentially provide more valuable clinical information for evaluation of cancerous diseases than independent systems alone.

Brief Description of Methodologies

The fully-3D SPECT subsystem permits complex acquisition trajectories around the breast to avoid physical hindrances, overcome distortions due to inadequate sampling, and allow detection of lesions in the chest wall. The CmT subsystem, restricted to circular rotation, has an offset geometry to allow imaging wide range of breast sizes. The quasi-monochromatic cone-beam x-ray source allows for reduced radiation dose and increased contrast between similar soft tissue attenuation coefficients. Geometric and anthropomorphic phantoms using fiducial markers were acquired to study the sampling/resolution properties and demonstrate image fusion. In addition, a preliminary investigation on the clinical performance of the hybrid system was done by imaging a woman with confirmed breast cancer.

Results

Images of geometric and breast phantoms were easily registered despite the slight distortion and artifacts in CmT images which possibly resulted from insufficient sampling due to the tilted and offset geometry. The initial hybrid imaging human subject study showed that SPECT images can easily see through the chest wall. Physical system constraints limited visualization of the chest wall in the CmT images, which can potentially be overcome with improved patient positioning (Fig. 2).

Conclusions (potential impact on breast cancer research and/or treatment)

The implementation of this first dedicated SPECT-CmT system promises greatly improved visualization in the detection/staging of cancer and the monitoring of treatment therapies.

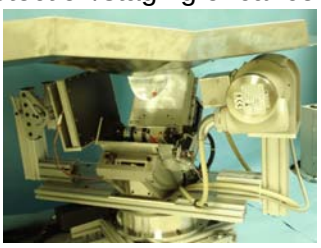

Fig. 1: Prototype hybrid SPECT-CT system with customized patient bed

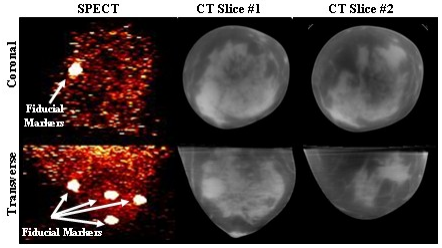

Fig. 2: Recons of the (LEFT) SPECT (MIP image), and (MIDDLE, RIGHT) CT slices of the left breast.

Presented at the
2008 Era of Hope Meeting
Baltimore, Maryland
25-28 June, 2008

interchangeably. **Conclusion:** The comparison of the normalized $IAUC_{60}$ showed that both DCE-CT and -MR imaging modalities may be used interchangeably in assessing cervical cancers. The normalized $IAUC_{60}$ may be considered as a reliable quantitative surrogate of the normalized transfer constant for both modalities.

TU-C-332-02

Concomitant Segmentation and Registration of Liver Anatomy Using SPECT-CT Imaging

T Fox*, E Schreibmann, I Crocker, Emory UniversitySchool of Medicine, Atlanta, GA

Purpose: To develop an automatic and accurate technique for concomitant segmentations and registration of liver anatomy using SPECT and CT images for unsealed source radiotherapy. **Method and Materials**: The link between segmentation and registration is given by the using the level set of a liver segmentation into the registration process. In the combined approach, the liver is automatically segmented from the CT image by evolving an initial seed with a level set until it locks to the liver's border as observed in the CT images. The time-crossing map of the level set is then used to match gradients in the SPECT image to the level set by using a data structure containing the signed distance values at a small band of neighboring pixels. **Results:** The technique was applied to three cases of metastatic liver disease treated with unsealed source therapy. Results indicated that the speed map of the level set plays an importance role in obtainng an accurate registration and produce a segmentation that is superior in registration time and accuracy over manual segmentation or the standard registration approach using mutual information. Accuracy measured with the convergence analysis method was of less than 0.5 mm rotation and 1 degree rotation. **Conclusion:** With the proposed combined segmentation-registration technique, the uncertainty of soft-tissue target localization could be greatly reduced ensuring accurate therapy assessment to be precisely delivered as planned. The combined all-in-one approach is automated and provides excellent accuracy over manual segmentation and mutual information approaches.

TU-C-332-03

Automatic Definition of Radiation Targets Using Textural Characteristics of Both Co-Registered PET and CT Images

C Caldwell[1], K Mah[2], H Yu[3]*, (1), Odette Cancer Centre at Sunnybrook Health Science Center, ON, CA, (2) Toronto Sunnybrook Cancer Ctr, Toronto, ON, CA, (3) Univeristy of Toronto, Toronto, ON, CA

Purpose: To automatically segment the radiation target for treatment of head and neck cancer (HNC) from FDG-PET/CT images using a textural classifier and to compare the automated results with contours defined by expert observers. **Method and Materials**: 27 image features, including textural features from Spatial Gray-Level Dependence Matrices and Neighborhood Gray-Tone-Difference Matrices, as well as statistical and structural features were calculated for 476 head and neck regions of interest (ROIs) in PET/CT images of 20 patients with HNC and 20 patients with lung cancer. A voxel based automated segmentation method using a Decision Tree (DT) based K nearest neighbors (KNN) classifier was developed based on the features in these ROIs. PET/CT images of another 10 head and neck patients who had all primary tumors and positive nodes manually segmented by three radiation oncologists were used to evaluate the method. Features were calculated for each voxel from corresponding PET and CT images within a window centered on the voxel. All voxels of head and neck soft tissues from the below the eye to the apex of the lung were automatically segmented. **Results**: The specificity was 95% ± 2% when all "true negative" voxels were considered to be all soft tissue voxels excluding the ROIs considered abnormal by one or more of three radiation oncologists. Sensitivity was 84% ± 19% when "true positive" was considered the intersection of at least two physicians' abnormal ROIs and sensitivity was 90% ± 16% when all "true positive" was the intersection of the abnormal ROIs of all three physicians. **Conclusion:** This work suggests that an automated segmentation method based on texture classification of FDG-PET/CT images has potential to provide accurate delineation of HNC. This could potentially lead to reduction in inter-observer variability in target delineation and improved accuracy of treatment delivery.

TU-C-332-04

Pilot Patient Studies Using a Dedicated Dual-Modality SPECT-CT System for Breast Imaging

P Madhav*, S Cutler, D Crotty, K Perez, R McKinley, P Marcom, T Wong, M Tornai, Duke University Medical Center, Durham, NC

Purpose: Acknowledging the limitations/discomfort of mammography has inspired the development of a dedicated SPECT-CT system to detect breast cancer, monitor therapeutic responses, and improve patient comfort. This system provides semi-quantitative 3D functional/anatomical imaging of a pendant, uncompressed breast. Fused images can potentially provide more valuable clinical information than independent systems alone. **Method and Materials:** The SPECT subsystem permits fully-3D complex acquisition trajectories around the breast, avoiding physical hindrances, overcoming distortions due to inadequate sampling, and allowing lesion detection on the chest wall. The CT subsystem, restricted to circular rotation, uses a quasi-monochromatic, cone-beam x-ray source, which allows for reduced radiation dose and increased contrast between similar soft tissue attenuation coefficients. With no breast compression and an open, common field-of-view geometry system, the patient lies prone on a customized patient bed while the hybrid device non-invasively acquires 3D data underneath. A preliminary investigation on the clinical performance of the hybrid system was done by imaging women with biopsy confirmed breast cancer **Results:** SPECT patient images can clearly visualize the tracer uptake by the tumor and view into the chest wall. Physical system constraints limit chest wall visualization in the CT patient images and thus patient positioning is under modification. Eliminating overlapping tissues through 3D imaging, the CT images improve lesion isolation versus 2D imaging modalities. Complementary functional and anatomical image information helps localize suspicious areas for subsequent analysis. **Conclusion:** Implementation of the world's first dedicated SPECT-CT system promises greatly improved visualization of the 3D breast volume. Complementary information from functional and anatomical imaging can guide lesion localization for subsequent analysis. **Conflict of Interest:** MPT is an inventor of this technology, and is named as an inventor on the patent for this technology applied for by Duke. If this technology becomes commercially successful, he and Duke could benefit financially.

TU-C-332-05

Simulation of Ultrasound Two-Dimensional Array Transducers Using a Frequency Domain Model

M Rao*, T Varghese, J Zagzebski, University of Wisconsin-Madison, Madison, WI

Purpose: Ultrasound imaging with two-dimensional (2D) arrays has garnered broad interest from scanner manufacturers and researchers for real time three-dimensional (3D) imaging. Previously we described a frequency domain B-mode imaging model applicable for linear and phased array transducers. In this study, we extend this model to incorporate 2D array transducers. **Method and Materials:** The pressure field for a 64×64 square array with element dimension of 0.15 mm and center-to-center spacing of 0.2 mm was calculated by applying the paraxial approximation to solve the 2D Rayleigh integral. We assume a rigid baffle, no apodization, a 2.5 MHz center frequency, and a speed of sound of 1540 m/s. A single transmit focus at 30 mm and dynamic receive focus with an F-number of 2 was utilized. The 2D array model is compared with the widely used ultrasound simulation program FIELD II, which utilizes an approximate form of the time domain impulse response function. **Results:** Discrepancies between waveforms computed using our model and FIELD II are less than 4%, regardless of the steering angle for distances greater than 2 cm, yet computation times are on the order of 1/35 of those using FIELD II. Modern beam-forming techniques such as apodization, dynamic aperture, dynamic receive focusing and 3D beam steering can also be simulated. The simulated beam patterns and point spread function images allow evaluation of beam properties for specific transducer parameters. Simulations of B-mode images provide vivid demonstrations of the ability of 2D arrays with specific imaging parameters to detect lesions of a given backscatter contrast and size. **Conclusion:** The frequency domain approach provides an effective and feasible tool to model transmitted and pulse-echo fields as well as B-mode images for 2D array transducers.

Presented at the
50th Annual Meeting of the American Association of Physicists in Medicine
Houston, TX
27-31 July, 2008

Characterizing the MTF in 3D for a Quantized SPECT Camera Having Arbitrary Trajectories

Priti Madhav, *Member, IEEE,* James E. Bowsher, *Member, IEEE, IEEE,* Spencer J. Cutler, *Member, IEEE,* and Martin P. Tornai, *Senior Member, IEEE*

***Abstract*— The emergence of application-specific 3D tomographic small animal and breast imaging systems has stimulated the development of simple methods to quantify the spatial resolution or Modulation Transfer Function (MTF) of the system in three dimensions. Locally determined MTFs, obtained from line source measurements at specific locations, can characterize spatial variations in the system resolution and can help correct for such variations. In this study, a method is described to measure the MTF in 3D for a compact SPECT system that uses a 16x20cm^2 CZT-based compact gamma camera and 3D positioning gantry capable of moving in different trajectories. Image data are acquired for a novel phantom consisting of three radioactivity-filled capillary tubes, positioned nearly orthogonally to each other. These images provide simultaneous measurements of the local MTF along three dimensions of the reconstructed imaged volume. The usefulness of this approach is shown by characterizing the MTF at different locations in the reconstructed imaged 3D volume using various (1) energy windows; (2) iterative reconstruction parameters including number of iterations, voxel size, and number of projection views; (3) simple and complex 3D orbital trajectories including simple vertical axis of rotation, simple tilt, complex circle-plus-arc, and complex sinusoids projected onto a hemisphere; and (4) object shapes in the camera's field of view. Results indicate that the method using the novel phantom can provide information on spatial resolution effects caused by system design, sampling, energy windows, reconstruction parameters, novel 3D orbital trajectories, and object shapes. Based on these measurements that are useful for dedicated tomographic breast imaging, it was shown that there were small variations in the MTF in 3D for various energy windows and reconstruction parameters. However, complex trajectories that uniformly sample the breast volume of interest were quantitatively shown to have slightly better spatial resolution performance than more simple orbits.**

***Index Terms*—mammotomography, modulation transfer function, CZT detector, emission imaging, single photon computed emission tomography, three-dimensional trajectories**

Manuscript received August 15, 2008. This work was supported by NIH R01-CA096821, and in part by DOD W81XWH-06-1-0791 and DAMD17-03-1-0558, and NIH EB001040-01.

P. Madhav (e-mail: priti.madhav@duke.edu), S.J. Cutler and M.P. Tornai are with the Multi-Modality Imaging Lab in the Department of Radiology at Duke University Medical Center, and the Department of Biomedical Engineering at Duke University; J.E. Bowsher is with the Department of Radiation Oncology, Duke University Medical Center, Durham, NC 27710 USA

I. Introduction

THE Modulation Transfer Function (MTF) can be used to characterize the frequency composition of spatial resolution. For emission imaging, the MTF can be determined via the line spread function (LSF) from images of a line source [1] (i.e. a capillary tube filled with radioactivity) or an edge source (i.e. radioactivity placed behind a lead plate) [2] in air. Measurements are usually taken at various distances from the camera face to determine spatial variations in resolution. MTF variations with respect to object-to-background ratio contribute to characterizing system linearity. Knowledge of these variations in the spatial resolution of an imaging system is important in understanding the reliability of information derived from an image, (i.e. gauging the minimum size of a lesion that could be detected).

In emission tomography, spatial resolution is determined quantitatively by measuring the LSF or point spread function (PSF), and semiquantitatively by assessing the reconstructed image quality of standard test objects such as the 3D disk and frequency-resolution (cold or hot) rod phantoms. In 2D, measurements of the LSF or PSF often assume that radiation detectors have a continuous response across their surface that is invariant within any given plane parallel to the detector's surface. However, this invariance assumption is questionable for recent medium- and small-field-of-view nuclear emission cameras having quantized detector elements, as are assumptions of approximately Gaussian response. Parallel hole or pinhole collimation, e.g. for small-animal imaging, involves significant nonstationarity in gamma camera response. It is also more common to describe the system performance in the frequency domain by obtaining the Fourier Transform of the PSF or LSF. Generally, image filtering is done in frequency space. The noise power spectrum (NPS), detective quantum efficiency (DQE), and other common parameters used in describing system response are also all measured in the frequency domain and require the MTF in their calculations. Thus, there are various reasons for computing the MTF instead of simply the PSF or LSF. Therefore, by looking at the frequency response, measurement of the MTF in 2D or 3D can provide a quantitative insight into the full frequency response of the system regardless of the detector response function.

Previous line-source phantoms used to measure the MTF in

3D have been limited to measuring the spatial resolution one dimension at a time [3-5]. Arrays of point sources have also been used to assess spatial resolution in three dimensions at various locations throughout the image volume [6]. However, unlike line sources, 3D arrays of point sources are more difficult to manufacture and position uniformly, and also are more difficult to evaluate under different scatter and scatter-free conditions due to the nature of their support structure. For this work, a novel phantom was constructed to fully evaluate the three-dimensional MTF along three nearly orthogonal axes after a single tomographic acquisition. This phantom allows for the characterization of spatial resolution in three dimensions and at various locations throughout the imaged volume, providing insight into the total amount of blur and its spatial variation. This phantom can be especially useful for tomographic imaging systems capable of fully-3D acquisitions for SPECT or PET, though it could also be modified for use in transmission imaging systems [7].

Over the past few years, our laboratory has developed a dedicated emission mammotomography system [8-11]. Several 3D, non-traditional, noncircular trajectories about a pendant breast with various lesion sizes located in different areas have been implemented and assessed [9, 12]. Due to the spatially varying spatial resolution in SPECT and the nonlinear response of iterative ordered-subsets expectation maximization (OSEM) reconstruction, the system blur cannot be fully described by a single LSF or MTF. Instead, some indication of system blur can be provided by measuring the blur at several locations in the image, for several signal-to-background ratios, and for several sizes and shapes of structures of interest.

The purpose of this study is to describe the novel phantom and to use this phantom to characterize the local MTF in 3D and to identify parameters that can affect the overall spatial resolution of our current SPECT system. Here we focus on measuring the MTF in different locations in the 3D volume using several different energy windows, different reconstruction parameters and acquisition trajectories, and different object shapes. In the present paper, LSF refers to the image of a line source in zero background and at a particular location. MTF refers to the absolute magnitude of the Fourier Transform of a particular LSF (i.e. at a particular location in the image) and thus throughout this paper the MTF will be referred to as the local MTF. In addition, isotropic in this paper is defined in terms of the MTF being uniform throughout the entire volume.

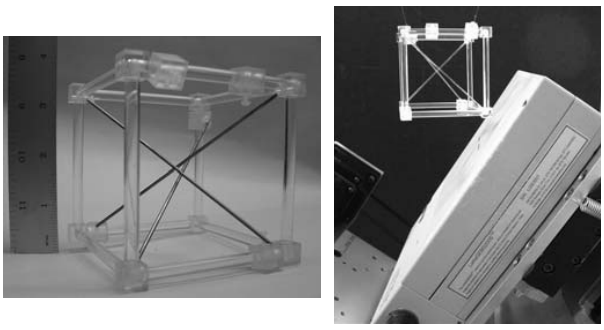

Fig. 1: (LEFT) Photograph of the acrylic phantom frame with three brass rods (brass rods were used in place of capillaries for the photo to clearly display the position of each tube). (RIGHT) Photograph of the phantom suspended in front of the compact SPECT camera in air during a 360° acquisition.

II. Materials & Methods

A. MTF Phantom

In order to quantify the spatial response of any imaging system including detector response, image acquisition procedures, complex 3D trajectories, scatter, and photon attenuation, a novel phantom was constructed (Fig. 1) to measure the local MTF in 3D. This phantom could be used for both emission (SPECT, PET, or even MRI) and transmission (x-ray CT) systems [7, 13]. A line source was chosen from which to obtain the MTF, since a radioactivity-filled capillary tube for emission imaging and solid tungsten wire for transmission imaging are easily interchangeable. Thus, this phantom would allow using a similar acquisition and quantification procedure for most imaging systems. More than one line source was necessary such that the MTF could be measured at different locations in the reconstructed imaged volume after a single tomographic acquisition. Using too many lines sources runs the risk of creating an overlap between the line sources in the reconstructed images, and so three lines were chosen. Additionally the phantom had very low scatter and attenuation characteristics, could be easily assembled, could be placed in any desired position in the camera's field of view, could be inserted into various fluid filled containers, and could provide flexibility to reposition the line sources in order to image anywhere in the imaged volume.

Based on the desired features, acrylic rods (side length of 7.8cm) are attached together into the shape of a box frame. Three capillary tubes (~11cm long with 0.9mm inner diameter) filled with 44.4-66.6MBq of aqueous ^{99m}Tc (140keV) were placed within the boxed frame such that each tube was held from one vertex to its corresponding opposite end, slightly away from another vertex. On its corresponding opposite end, the tube is attached to a slider piece which gives the flexibility to position the tube anywhere along the length of the side-rod to which it is attached. Depending on the size of the SPECT system, pixel size of the camera, and its minimum radius of rotation, smaller or larger capillary tubes could be used to encompass the entire field of view. The tubes were visibly separable in their positions such that they did not touch one another, and spanned the entire field of view. Also, they were not placed at exactly orthonormal planes in order to avoid potential aliasing.

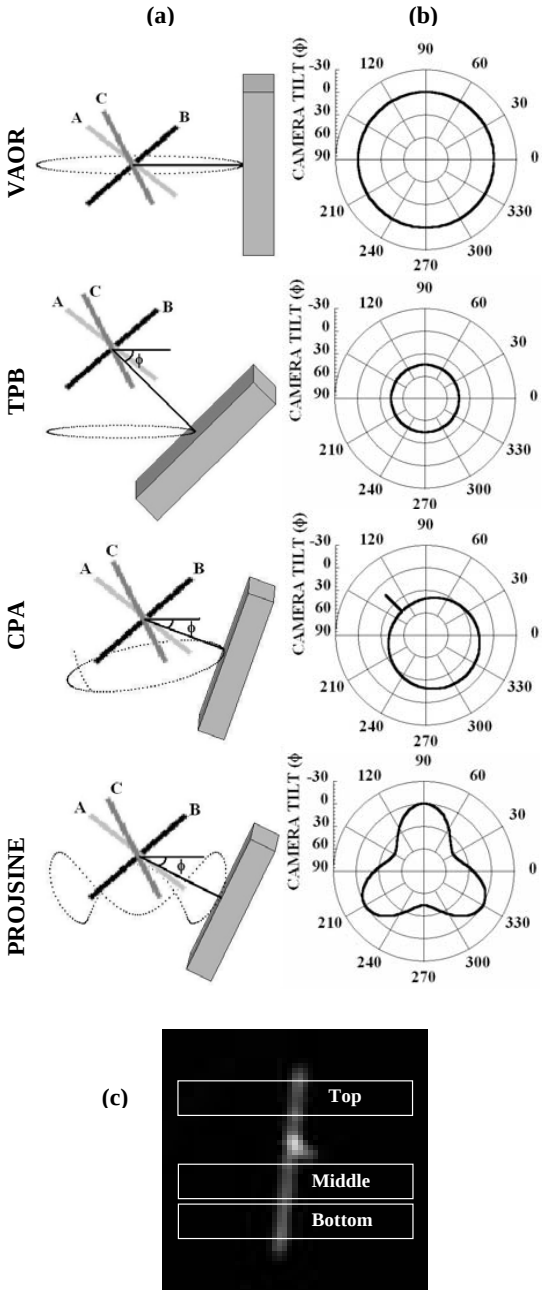

Fig. 2: (a) 3D setup of the phantom for all four trajectories. The SPECT camera (shown as a gray square) is facing left towards the phantom, placed at the center of the field-of-view. The phantom consists of three radioactivity-filled capillary tubes (labeled A,B,C). The shown placement of the tubes nearly matches the photograph of the phantom suspended in front of the SPECT camera in Fig. 1. The direction of increased polar camera tilt, φ, is also shown relative to the horizon. (b) Next to each 3D schematic is the corresponding polar plot (i.e. camera tilt) of the camera trajectory (plotted as a radius with +90° at the center and -30° at the edge) versus azimuth angle (plotted around the circle from 0° to 360°). (c) Reconstructed slice (5th iteration, 8 subsets, 80x80x80 grid size, 2.5mm) for one isolated capillary tube located in air acquired with a TPB orbit. "Top", "Middle, and "Bottom" of the capillary tube are defined for subsequently presented results, and span 11cm along the length of the line source.

B. Data Acquisition and Image Reconstruction

Our emission tomography system is composed of a compact 16x20cm^2 field of view cadmium zinc telluride (CZT) LumaGEM 3200S^{TM} gamma camera (*Gamma Medica, Inc.*, Northridge, CA) attached to a hemispherically positioning gantry. The camera uses a 64x80 array of 2.5x2.5x6mm^3 quantized CZT elements for a total of 5120 pixels. Measured mean energy resolution of the gamma camera at 140keV is 6.7% FWHM and overall sensitivity is 37.9 cps/MBq [11]. A parallel-hole collimator with hexagonal holes (1.2mm hole size flat-to-flat (inner diameter), 0.2mm septa, and 25.4mm

TABLE I

TRAJECTORY PARAMETERS USED FOR EACH ACQUISITION OVER A 360° AZIMUTHAL RANGE

Trajectories	Acronym	Number of Projs	Polar Tilt Range (min-max degrees)	ROR Range (min-max cm)
Vertical Axis of Rotation	VAOR	128	0°	8.74
Tilted Parallel Beam	TPB	128	45°	4.05
Circle Plus Arc	CPA	139	0°-45°	4.05-6.48
Three-Lobed Sinusoid Projected onto a Hemisphere	PROJSINE	150	15°-45°	4.05-8.74

Fig. 3: Photographs of the MTF phantom contained inside (LEFT) the 1000mL cylinder and (RIGHT) 850mL breast. (BOTTOM) Phantom was immersed in the water to the extent possible to quantify the effect of scatter along with various acquisition trajectories on the MTF, and (TOP) is also shown in the phantoms without water present.

height) is used in these studies. Due to the flexible gantry, the camera can be positioned anywhere in a hemisphere to facilitate acquiring projection data around a pendant uncompressed breast [8, 9, 11, 12].

Projections were collected over a 360° azimuthal rotation around the phantom suspended in air (Fig. 1 and Fig. 2(a)) using a vertical axis of rotation (VAOR), comparable to the simple circular orbits used by clinical SPECT systems (about their horizontal axis). Acquisitions were made at a radius of rotation (ROR) that corresponded to the minimum ROR possible when the MTF phantom was placed in different object shaped media (described in the next section). Data was collected in list mode and post-processed to obtain ±4% and ±8% wide symmetric energy windows about the 140keV photopeak. Total scan time for each acquisition was 10min, with increased acquisition times for subsequent scans to compensate for radioactive decay. Under these conditions, there were ~28k events per projection in the ±8% wide energy windowed data.

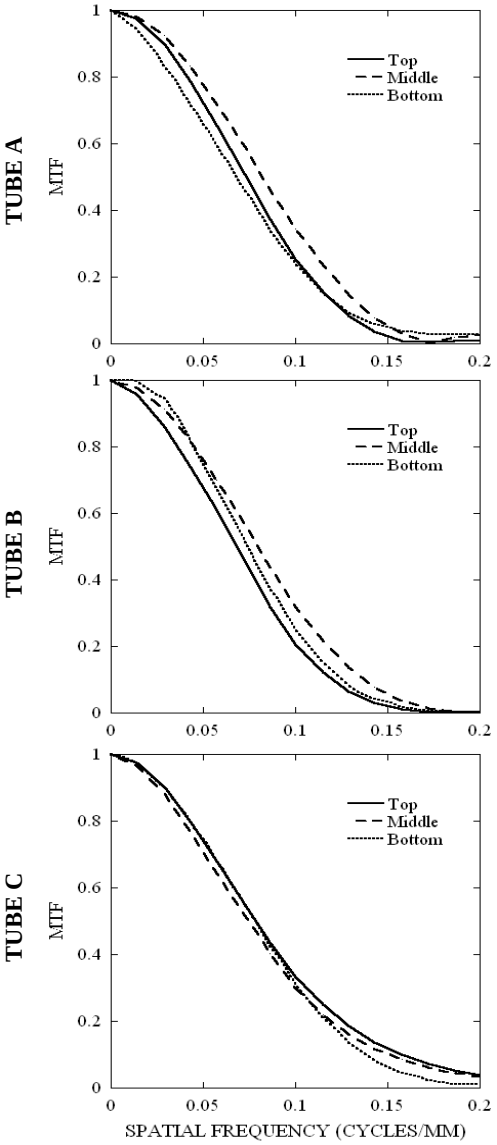

Fig. 4: Results for tube A (TOP), B (MIDDLE), and C (BOTTOM) show little variation in MTFs along different portions along the capillary line source for a 360° SPECT acquisition. MTF measurements were obtained from measurements taken of the phantom in air using a simple VAOR orbit. Nyquist frequency is at 0.2mm^{-1}.

Images were iteratively reconstructed using 8 subsets of OSEM, and displayed at 1, 3, 5, and 10 iterations in all cases. These reconstructions were on a grid of 80x80x80 voxels, for two different voxel widths – 1.25mm and 2.50mm. The reconstructions were performed using the same ray-driven code as described earlier in [9,10].

Three other trajectories were investigated: (1) tilted parallel beam (TPB) with 45° fixed camera tilt; (2) tilted circle plus (one) arc (CPA) with 45° max camera tilt, and (3) a three-lobed sinusoid projected onto a hemisphere (PROJSINE) with 0° to 45° polar camera tilting range (sinusoidal amplitude). These trajectories have been investigated elsewhere [9, 11, 12], but not for their frequency response characteristics. These trajectories and the direction of polar camera tilt are illustrated in Fig. 2. Specific parameters that were used for all four trajectories are given in Table I. The increased number of projections is due to the use of polar (ϕ) sampling along with azimuthal (θ) sampling, necessitating $\Delta\phi$ steps along with $\Delta\theta$ steps to reach 360º azimuthally.

C. MTF Phantom in Different Object Shapes

The degrading effects of different object shapes on the MTF were also evaluated by placing the line source phantom in two different environments: 1000mL water-filled glass-walled cylinder (12cm diameter) and 850mL water-filled plastic-walled breast-shaped container (nipple-to-chest distance of 11cm, medial-lateral distance of 17cm, and superior-inferior distance of 18cm) (Fig. 3). All four trajectories were investigated except for the cylinder where only VAOR was used. The local MTF was calculated for all trajectories measured with the phantom placed in the cylinder and breast. Data was collected using an ±8% wide symmetric energy window and was post-processed to also obtain ±4% wide symmetric energy windows. Energy window width for dedicated, uncompressed breast imaging has been shown to affect image quality under various acquisition conditions [14]. The 16% wide energy window, while not exploiting the fine resolution capability of CZT (6.7% intrinsic FWHM), corresponds to that used in standard, clinical nuclear medicine camera systems (15% wide), and is substantially narrower than that of scintillator based compact, quantized detector element gamma cameras (30% wide). Furthermore, early contrast-detail observer studies with this system have shown that energy windows near but above the intrinsic system resolution allow for visualization of small objects [14]. The ROR was determined by placing the breast 1cm or less away from the camera face at all camera orientations. For all four trajectories tested, acquisitions were obtained at the same

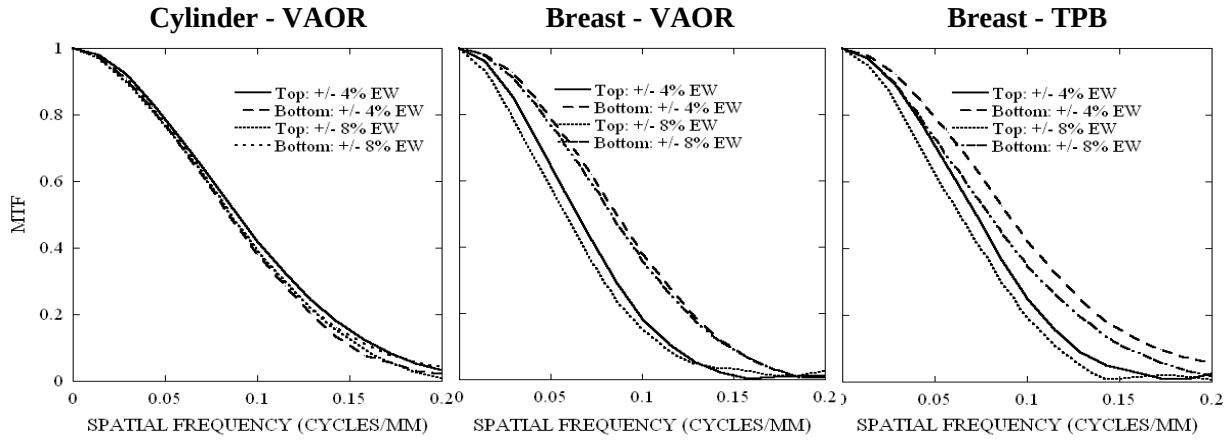

Fig. 5: MTF of the top and bottom segment of the capillary source B placed in a water-filled cylinder (LEFT) and a water-filled breast shape phantom acquired using VAOR (MIDDLE) and TPB (RIGHT) orbits at ±4% and ±8%energy windows. Smaller energy windows appear to not have a significant effect on resolution.

RORs used for the phantom in air (shown in Table I). Scans were also performed over 10min, with increased acquisition times for subsequent scans to compensate for radioactive decay. Under these conditions, approximately 13k counts were collected in each ±8% wide energy windowed projection of the MTF phantom measured in the scatter media. Iterative reconstruction was performed using the same parameters for the projections of the phantom suspended in air.

D. Local MTF Determination

The overall local MTF calculation was computed based on an algorithm presented elsewhere [15], and has been successfully applied in the preliminary local MTF measurements of our 3D x-ray computed mammotomography (CmT) system as well [7]. Once the images were reconstructed, the first step was to manually rotate the images such that each tube could be isolated onto a single slice (Fig. 2, (c)). A binary line image of the outline of the tube was acquired by using a Sobel edge detection method [16]. The angle and position of the tube was determined by the Radon transform. Based on the resulting curves in polar coordinate space, the location of the curves' intersection (i.e. maximum intensity) gave an estimate of the angle and spatial position of the line source [17]. Inaccuracy in estimating the true angle of a line can give an unsmooth LSF and degrade the MTF, especially in higher frequency regions. A composite local LSF was generated by reprojecting and resampling a small region of interest around the line source onto a one-dimensional array of sub-pixel bins positioned perpendicular to the calculated angle of the tube. Use of subpixel bins was necessary since the samples were not uniformly distributed along the one-dimensional array [18]. Different subpixel bin sizes (0.1, 0.3, and 0.7) were initially tested to find an optimal bin size. For smaller bin sizes, such as 0.1, high frequency components were exaggerated in the MTF due to the increased noise. At larger bin sizes, such as 0.7, the zero of the MTF occurred below the Nyquist frequency. Therefore, for this work 0.3 subpixel bin size was found to the optimal size. The samples were thus binned to 1/3 of the original pixel size of 2.5mm. This result was then smoothed by averaging neighboring pixels within a three pixel moving average window to get the final local LSF (LSF_f):

$$LSF_f(x) = \frac{LSF(x-1) + LSF(x) + LSF(x+1)}{3} \qquad (1)$$

where x is the spatial location of the pixel. Smoothing is necessary to reduce the noise and effect of the high-frequency response in the MTF. Zero padding and a Hanning filter were also applied to the local LSF to eliminate other high frequency artifacts.

Corresponding local MTFs were calculated by taking the absolute value of the one-dimensional discrete Fourier Transform of the LSF_f.:

$$MTF(f) = \left| \Im\{LSF_f(x)\} \right| \qquad (2)$$

where f represents the spatial frequency. The local MTF here describes the magnitude of the component response of the system to the known input. Since an infinitely small line source is not being used, the effects of the finite width of the capillary tube, a, is corrected for by dividing the MTF by a sinc $(\pi a f)$. This MTF was finally normalized to yield the final MTF. The MTFs along various parts of the tube (e.g. a "local MTF") were calculated in order to evaluate the response at different locations in the sampled volume (Fig. 2, (c)).

For each tube, an average MTF, its standard deviation, and upper and lower bounds for the estimated average MTF was calculated from the measured MTF along different segments of the tube. Using these results, the root mean square difference (RMSD) was calculated by subtracting the upper

and lower bounds, squaring the difference, finding the average of all these squared differences, and taking the square root. The measured RMSD values help to evaluate the amount of uniformity in the MTF along different portions of a single line source.

III. Results & Discussion

A. MTF Along Different Line Location

Fig. 4 shows the local MTFs measured in air with the 16% wide energy window at different locations along each of the nearly orthogonal capillary tubes. Measurements were derived from images collected of the phantom in air using the VAOR orbit. For all three orientations, there was only a small variation in the MTF along the lines, indicating uniform 3D resolution throughout the imaged volume. VAOR orbits are known to be the largest uniformly sampled volumes for both conventional and compact, versatile 3D SPECT cameras [9]. The uniformity of these results is not surprising since the SPECT scan was collected over a 360° azimuthal orbit. Hence, projection "averaging" throughout this reconstructed volume may be expected to yield a nearly uniform response.

B. MTF at Different Energy Window

The MTF was also determined at ±4% and ±8% energy windows to see if different amounts of object scatter would affect the resolution of the reconstructed images. Fig. 5 shows the MTF for one of the capillary tubes in the MTF phantom suspended in the water-filled cylinder and the water-filled

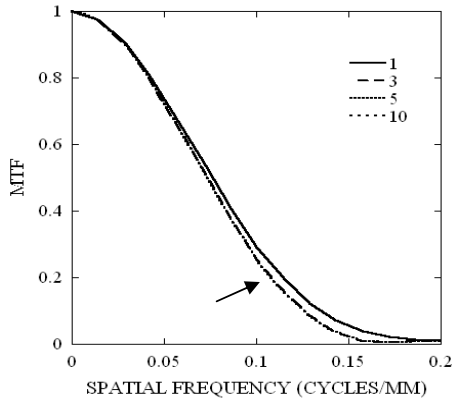

Fig. 6: MTF at several iterations of the phantom in air using VAOR. MTFs overlap for iterations 3, 5 and 10 (shown by arrow). MTF was obtained using the top portion of capillary A.

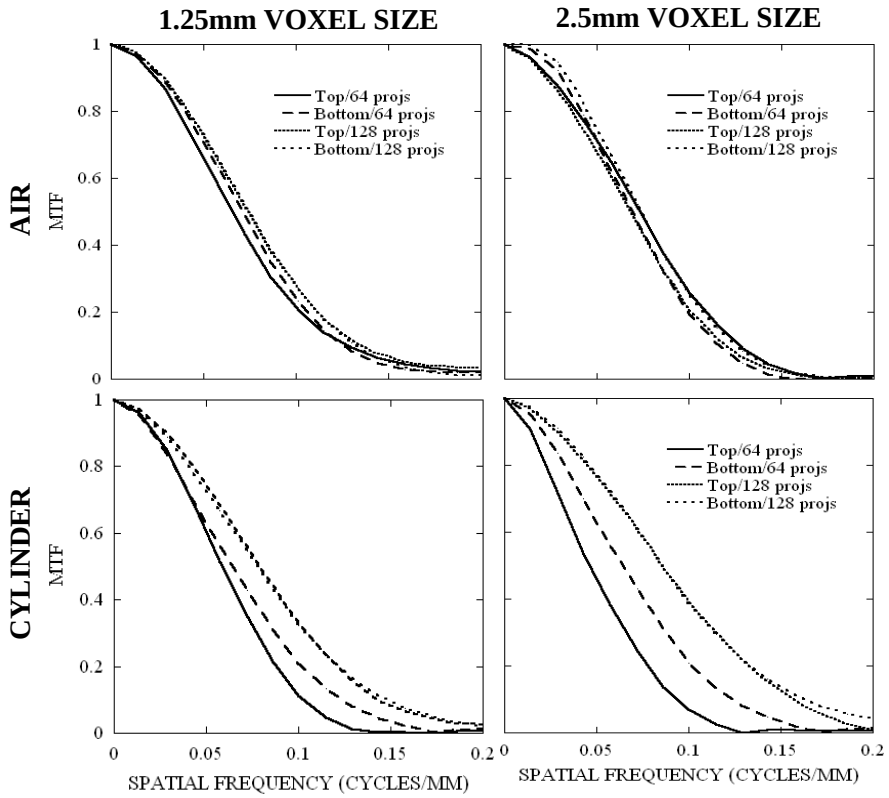

Fig. 7: (TOP ROW) MTF obtained of the phantom in air at a reconstructed voxel size of (LEFT COLUMN) 1.25mm (160x160x160 grid size) and (RIGHT COLUMN) 2.5mm (80x80x80 grid size). Plots indicate very slight difference between the different numbers of indicated projections. (BOTTOM ROW) Unlike in air, the MTF obtained from the phantom in the water-filled cylinder, for both voxelizations, has a greater decrease and more anisotropy in MTF for the 64 projection data set. MTFs shown here were obtained using capillary tube B and VAOR orbital acquisition (see Fig. 2).

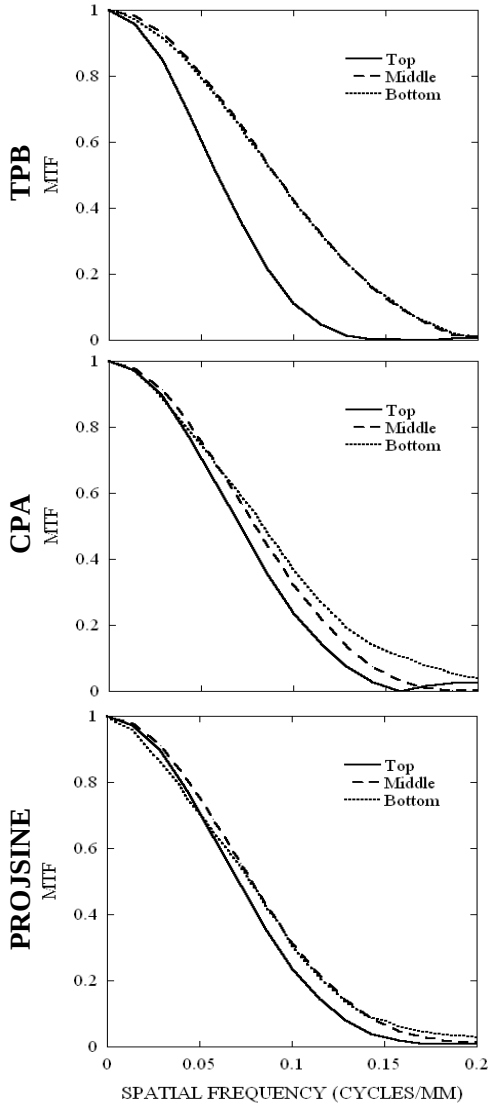

Fig. 8: Using TPB (TOP), CPA (MIDDLE), and PROJSINE (BOTTOM) trajectories, the MTFs were obtained from the top, middle, and bottom segment of the reconstructed line source B. The MTFs for TPB and CPA have more variation among different segments along the tube compared to VAOR (Fig. 4, MIDDLE) and PROJSINE. For the bottom line segment, both TPB and CPA actually give a higher MTF than VAOR and PROJSINE due to the bottom segment being closest to the camera throughout the trajectory, as seen in the schematic in Fig. 2, (a).

breast, with data acquired using VAOR and TPB orbits at both energy windows. For the cylinder, there is no difference in the MTFs measured anywhere along the line.

For the breast phantom, the MTF results are somewhat different. There are differences in the measured MTFs at different locations, which correspond to the thicker posterior breast (top) or narrower anterior breast near the nipple (bottom), but no significant differences in these locations due to energy window width. Furthermore, using a smaller energy window with incomplete sampling and the TPB orbit also had a very slight effect on the local MTF.

TABLE II

RMSD VALUES FOR EACH CAPILLARY TUBE ACQUIRED USING VARIOUS TRAJECTORIES

Trajectories	Tube A	Tube B	Tube C
VAOR	0.049	0.044	0.039
TPB	0.145	0.123	0.042
CPA	0.103	0.093	0.091
PROJSINE	0.041	0.032	0.040

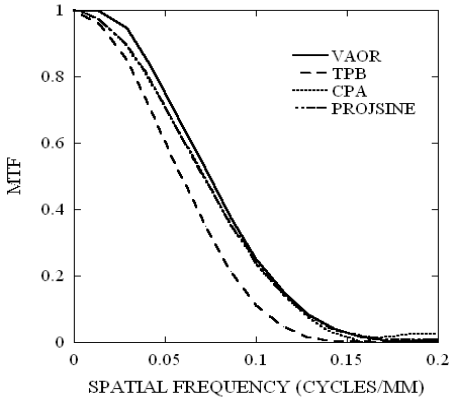

Fig. 9: The MTFs were obtained from the top segment of the reconstructed line source B for each of the three orbits. TPB produces slightly worse MTFs than VAOR and PROJSINE since the top segment is farther away from the camera for those trajectories.

C. MTF with Various Reconstruction Parameters

In OSEM, the projection data is grouped into subsets and the EM algorithm is applied to each subset to get an estimate of the image. In principle, more iterations are performed until the algorithm has converged to a true (or near) optimum value. However this can yield images of poor quality. Previous studies for emission mammotomography imaging breast lesions have shown that there is a trade-off between the rate of contrast improvement and SNR degradation in the reconstructed images [8, 9, 12]. This contrast-SNR roll-over is similar to the minimum of a bias-variance metric. For SPECT mammotomography imaging this roll-off is often best between 2 and 3 iterations.

In a similar way, the measured local system MTF appears to have stopped changing after only a few iterations. Fig. 6 shows the MTF at 1st, 3rd, 5th, and 10th iterations along a single dimension. The slow-down in MTF improvement is probably similar to the slow-down in contrast improvement with increasing iterations. At the 5th and 10th iteration, it appears that there is no change in the MTF beyond the 3rd iteration. The results are similar (not shown) for the other portions of each of the three capillary sources for a uniform orbit such as VAOR.

Using smaller voxel sizes and fewer projection images during iterative reconstruction can also have an effect on the measured resolution (Fig. 7). As voxel size decreases and number of projections increase, the MTF expectedly improves and remains consistent (less anisotropic), especially under non-ideal conditions (i.e. water-filled cylinder) (Fig. 7,

TABLE III

RMSD VALUES FOR EACH CAPILLARY TUBE IN BREAST ACQUIRED USING VARIOUS TRAJECTORIES

Trajectories	Tube A	Tube B	Tube C
VAOR	0.056	0.064	0.086
TPB	0.103	0.092	0.122
CPA	0.092	0.119	0.096
PROJSINE	0.050	0.052	0.046

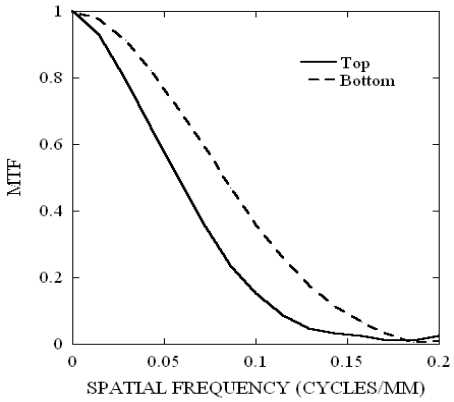

Fig. 10: MTF obtained from the line phantom (capillary tube B) placed in the breast using the VAOR orbit. Unlike MTF curves obtained in air and a cylinder, there is more variation in MTF in a breast phantom.

BOTTOM). From these plots, it can be inferred that when acquiring fewer projections under non-ideal conditions, the MTF varies significantly due to incompleteness of sampling the scatter distribution and can introduce artifacts in the reconstructed images. However, very small differences are seen in the MTF for conditions without scatter (Fig. 7, TOP). The MTF obtained at 128 projections in the water-filled cylinder appears to be better than in air. This could be due to the increased attenuation and noise in the scatter images which made it more difficult to localize the signal.

D. MTF with Various 3D Trajectories

Other than VAOR, three different trajectories, TPB, CPA, and PROJSINE, were also evaluated by measuring the MTF at three different locations along the capillary tube in air (Fig. 8). RMSD results in Table II indicate small but similar variations in the MTF for VAOR and PROJSINE. The importance of this is that the complex trajectory will likely be necessary for clinical breast imaging [8, 9], while VAOR provides a completely sampled region with the largest volume. The TPB and CPA trajectories yielded a worse MTF in the top portion, but had a better MTF at the bottom portion due to the relative position of the camera to the line sources (Fig. 8). This is most likely due to a combination of incomplete sampling, attenuation, and distance related degradations associated with SPECT imaging.

Fig. 9 shows the difference in spatial resolution among each of the four orbits for the top segment of the capillary tube. Previous studies have shown that insufficient sampling can cause the reconstructed slices to be distorted [9, 12]. For the TPB orbit, in contrast to the bottom segment of the capillary source, the top segment of the capillary tube (shown in schematic in Fig. 2, (a)) is never close to the face of the SPECT camera, causing a difference in the measured spatial response.

E. MTF within Different Object Shapes

Using a VAOR orbit, the MTF was determined for the line phantom suspended in (1) air; (2) a water-filled cylinder; and (3) a water-filled breast phantom using the same, fixed ROR for all three cases. Images reconstructed with 5 iterations and 5 subsets of an OSEM algorithm produced minimal differences between the MTF obtained in air and in the

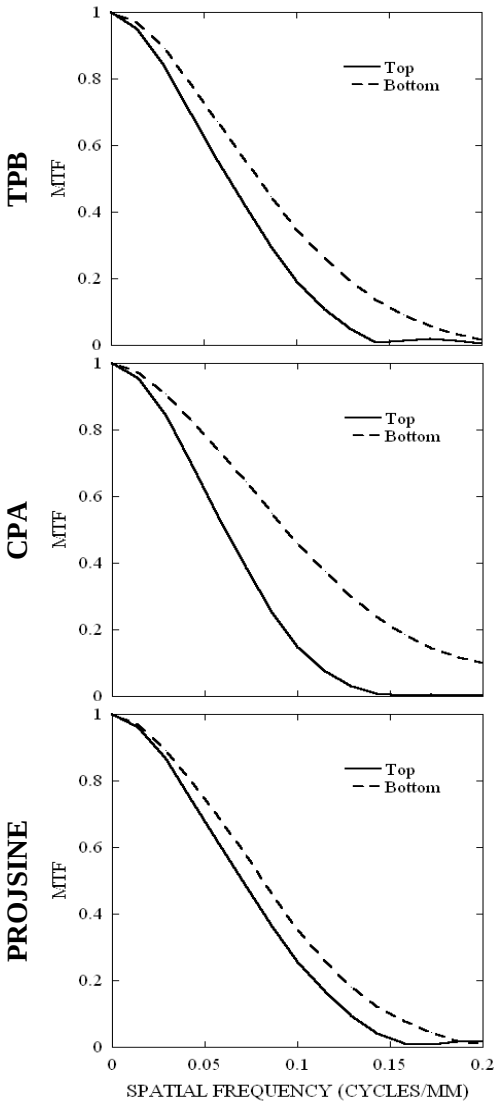

Fig. 11: MTF obtained from the phantom (top and bottom segment of capillary tube B) placed in the breast using TPB (TOP), CPA (MIDDLE), and PROJSINE (BOTTOM) trajectories. Results are very similar to results measured in air.

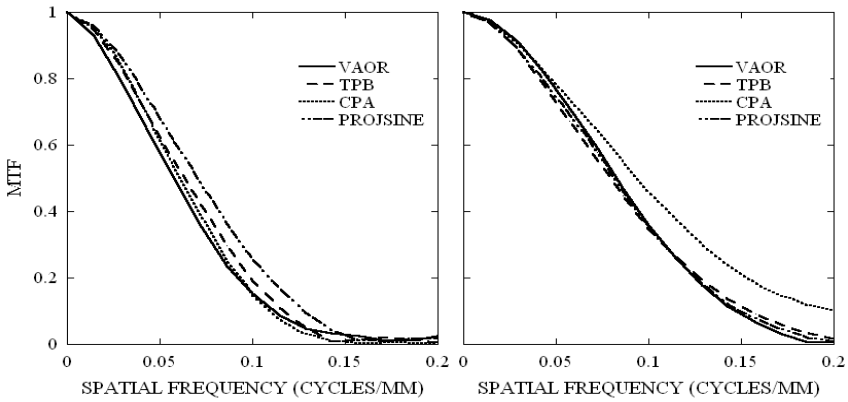

Fig. 12: MTF of the top (LEFT) and bottom (RIGHT) segment of capillary source B placed in the breast for all four trajectories.

cylinder (Fig. 4 and Fig. 7), but showed a slight difference in comparison to the MTF obtained with the breast phantom (Fig. 10) mostly likely due to the differences in object shape (i.e. breast phantom versus a cylinder) and a slight difference in the measured location relative to the measurement in air or with the cylinder. RMSD values for capillary tube B acquired in air, cylinder, and breast are 0.044, 0.048, and 0.064, respectively. This slight degradation in resolution seen with VAOR in a breast phantom illustrates the necessity of using novel trajectories that use increased camera tilt angles to improve sampling and also achieve a closer ROR. As shown in Fig. 10, Fig. 11 and Table III, there is slight variation in the MTFs with VAOR, TPB and CPA trajectories, consistent with earlier results using these trajectories. There is considerably less variation with PROJSINE. Comparisons of all four trajectories are plotted together for the top and bottom segment of the capillary tube (Fig. 12).

IV. Conclusions

In this work, we have developed a novel phantom for use in measuring the local MTF in 3D to evaluate versatile, novel-trajectory emission tomographic systems and provide an insight into the degrading effects caused by different orbital acquisitions, different shaped geometries, and the reconstruction process. This initial study demonstrated that energy window has a secondary effect on resolution, in contrast to incomplete sampling. The relatively small number of OSEM iterations also had little effect on the MTF, and that more projections are necessary in non-ideal conditions (i.e. with attenuation media) to yield an improved and more isotropic MTF. Also, it was shown that unlike for simple circular (VAOR) and more complex (PROJSINE) trajectories, asymmetric acquisition trajectories (e.g. TPB and CPA) have more variations in the MTF between different locations in 3D space. Differences between the curves are caused both by trajectories having fixed polar tilt and subsequently incomplete sampling. This implies that a complex trajectory like PROJSINE more uniformly samples the breast volume of interest and may be necessary for clinical breast imaging. Having flexible 3D positioning about the breast yielded minimal RMSD differences, which is important for high resolution molecular emission imaging.

This study also demonstrates the benefit of using a local 3D MTF phantom to evaluate a tomographic imaging system. With such a phantom, the effect of attenuation, scatter, energy windows, reconstruction process, and 3D trajectories can be easily evaluated to get a better understanding on how these different parameters can affect image quality.

Acknowledgement

The authors would like to thank Dr. Caryl Catarious and Dr. Ehsan Samei for their assistance in this project.

References

[1] M. L. Nusynowitz and A. R. Benedetto, "Simplified method for determining the modulation transfer function for the scintillation camera," *J. Nucl. Med*, vol. 16, pp. 1200-1203, 1975.

[2] T. Väyrynen, U. Pitkänen, and K. Kiviniitty, "Methods for measuring the modulation transfer function of gamma camera systems," *Eur. J. Nucl. Med.*, vol. 5, pp. 19-22, 1980.

[3] M. Coleman, M. A. King, S. J. Glick, K. Knesaurek, and B. C. Penney, "Investigation of the stationarity of the modular transfer function and the scatter fraction in conjugate view SPECT restoration filtering," *IEEE Trans. Nucl. Sci.*, vol. 36, pp. 969-972, 1989.

[4] S. J. Glick, M. A. King, K. Knesaurek, and K. Burbank, "An investigation of the stationarity of the 3D modulation transfer function of SPECT," *IEEE Trans. Med. Imag.*, vol. 36, pp. 973-977, 1989.

[5] S. J. Glick, W. G. Hawkins, M. A. King, B. C. Penney, E. J. Soares, and C. L. Byrne, "The effect of intrinsic attenuation correction methods on the stationarity of the 3-D modulation transfer function of SPECT," *Med. Phys.*, vol. 19, pp. 1105-1112, 1992.

[6] L. R. Furenlid, D. W. Wilson, Y. Chen, H. Kim, P. J. Pietraski, M. J. Crawford, and H. H. Barrett, "FastSPECT II: A second-generation high-resolution dynamic SPECT imager," *IEEE Trans Med Imaging*, vol. 51, pp. 631-635, 2004.

[7] P. Madhav, R. L. McKinley, E. Samei, J. E. Bowsher, and M. P. Tornai, "A novel method to characterize the MTF in 3D for computed mammotomography," *2006 SPIE Med Imag Conf*, vol. 6142, 11-17 Feb. 2006 2006.

[8] M. P. Tornai, J. E. Bowsher, C. N. Archer, J. Peter, R. J. Jaszczak, L. R. MacDonald, B. E. Patt, and J.S. Iwanczyk, "A 3D gantry single photon emission tomograph with hemispherical coverage for dedicated breast imaging," *Nucl. Instr. Meth. Phys. Res. A*, vol. 497, pp. 157-167, 2003.

[9] C. N. Archer, M. P. Tornai, J. E. Bowsher, S. D. Metzler, B. C. Pieper, and R. J. Jaszczak, "Implementation and initial characterization of

acquisition orbits with a dedicated emission mammotomograph," *IEEE Trans. Nucl. Sci.*, vol. 50, pp. 413-420, 2003.

[10] C. N. Brzymialkiewicz, M. P. Tornai, R. L. McKinley, S. J. Cutler, and J. E. Bowsher, "Performance for dedicated emission mammotomography for various breast shapes and sizes," *Phys Med Biol*, vol. 51, pp. 5051-5064, 2006.

[11] C. N. Brzymialkiewicz, M. P. Tornai, R. L. McKinley, and J. E. Bowsher, "Evaluation of fully 3D emission mammotomography with a compact cadmium zinc telluride detector," *IEEE Trans. Med. Imag.*, vol. 24, pp. 868-877, 2005.

[12] C. N. Brzymialkiewicz, M. P. Tornai, R. L. McKinley, and J. E. Bowsher, "3D data acquisition sampling strategies for dedicated emission mammotomography for various breast sizes," *2005 IEEE Nucl Sci Symp & Med Imag Conf*, vol. 4, pp. 2596-2600, 16-22 Oct. 2004 2004.

[13] P. Madhav, C. N. Brzymialkiewicz, S. J. Cutler, J. E. Bowsher, and M. P. Tornai, "Characterizing the MTF in 3D for a quantized SPECT camera having arbitrary trajectories using a novel phantom," *2005 IEEE Nucl Sci Symp & Med Imag Conf*, pp. 1722-1726, 23-29 Oct. 2005.

[14] S. J. Cutler, C. N. Brzymialkiewicz, and M. P. Tornai, "Investigating the effects of energy resolution in dedicated emission mammotomography," *2005 IEEE Nucl Sci Symp & Med Imag Conf*, vol. 5, pp. 2537-2541, 23-29 Oct. 2005 2005.

[15] E. Samei and M. J. Flynn, "A method for measuring the presampled MTF of digital radiographic systems using an edge test device," *Med. Phys.*, vol. 25, pp. 102-113, 1998.

[16] J. S. Lim, *Two-Dimensional Signal and Image Processing*. Englewood Cliffs, NJ: Prentice Hall, 1990.

[17] R. C. Gonzalez, *Digital Image Processing*, 2nd ed. Reading, Mass: Addison-Wesley, 1987.

[18] H. Fujita, D. Tsai, T. Itoh, K. Doi, J. Morishita, K. Ueda, and A. Ohtsuka, "A simple method for determining the modulation transfer function in digital radiography," *IEEE Trans. Med. Imag.*, vol. 11, pp. 34-39, 1992.

APPENDIX F: IEEE MRBC ABSTRACT

Improved Chest Wall Imaging through Combined Complex Trajectories in Dedicated Dual Modality SPECT-CT Breast Molecular Imaging

D. J. Crotty[1,2], S. J. Cutler[1,2], R. L. McKinley[3], P. Madhav[1,2], K. L. Perez[1,4], M. P. Tornai[1,2,4]
[1]*Dept. Radiology, Duke University Medical Center, Durham, NC, USA*
[2]*Dept. Biomedical Engineering, Duke University, Durham, NC, USA*
[3]*Zumatek Incorporated, Chapel Hill, NC, USA*
[4]*Medical Physics Graduate Program, Duke University Medical Center, Durham, NC, USA*

In the hybrid SPECT-CT breast molecular imaging system currently in development in our lab, patient positioning is a practical compromise between comfort and a need to maximize the imaged volume of breast and chest wall. While the integrated system rotates under the patient, the CT system is restricted to azimuthal trajectories at a fixed height, but the flexible SPECT system is capable of fully 3D positioning around the pendant breast. The current bed design separates the top of the CT cone beam from the chest wall, thus limiting the system's ability to image this area. This study examines combined complex trajectories, including limited angle tomography for both modalities and raising the entire imaging system during the scan, to more effectively image lesions in or near the chest wall. While emphasizing new CT system trajectories, novel asymmetrical SPECT trajectories are also developed to maximize the imaged volume while avoiding contact with the bed or patient. Various sized lesions filled with low and medium concentrations of 99mTc activity (10:1 to 3:1) and CT contrast are imaged using a range of trajectories. Dual modality projections are post-processed to mimic limited angle trajectories or trajectories that raise the CT system for a portion of the scan. Reconstructed image metrics including SNR, contrast, attenuation coefficients and lesion profiles are quantified to understand the effect of these trajectories; image registration effects are also examined in addition to the effect that raising the system has on acquisition sequencing for the orthogonally placed sub-systems. Initial reconstructed images from data sets with trajectories that removed 60° of SPECT and CT azimuthal data and trajectories combining limited angle acquisition with vertical system shift qualitatively show a significant increase in observed volume while maintaining lesion visibility. Simple system shifting in mid-scan thus appears to improve chest wall imaging for both modalities.

Presented at the
Fourth International Workshop on the Molecular Radiology of Breast Cancer (MRBC)
Dresden, Germany
20-21 October, 2008

APPENDIX G: IEEE MRBC ABSTRACT

Comparison of 2D Scintimammography and 3D Dedicated Breast SPECT Using a Compressible Breast Phantom and Lesions of Varying Size and Tracer Uptake

S. J. Cutler[1,2], K. L. Perez[1,3], P. Madhav[1,2], M. P. Tornai[1,2,3]
[1]*Department of Radiology, Duke University, Durham, NC, USA*
[2]*Department of Biomedical Engineering, Duke University, Durham, NC, USA*
[3]*Medical Physics Program, Duke University, Durham, NC, USA*

This study aims to quantitatively and qualitatively compare 2D planar scintimammography imaging of the breast under various degrees of compression with uncompressed, dedicated 3D SPECT using contoured acquisition trajectories. A 700mL compressible anthropomorphic breast phantom containing small lesions was developed to compare 2D and 3D breast imaging. Thin walled, deformable lesions from 40 to 500uL volume suspended on narrow tubing in the phantom were used to mimic breast lesions undergoing different degrees of compression. Using a 16x20cm^2 CZT-based gamma camera, ^{99m}Tc-scintimammography was performed for 10min imaging times for compression thicknesses from 6 to 12cm (fully uncompressed) using a single mediolateral view. Dedicated breast SPECT was then performed for 10min using the uncompressed breast acquired with a vertical axis of rotation, simple tilted rotation, and a complex 3D acquisition trajectory. Experimental variables include: (1) background torso contamination; (2) (in)homogeneous breast composition; and (3) low count (clinically relevant) and high count (low noise) images. The radioactivity lesion:background concentration ratio was varied from 12:1 down to 3:1. A comparison between the two modalities was made in a limited observer study with independent observers analyzing reconstructed images for the smallest detectable lesion. Image quality, based on lesion SNRs and contrasts, and sampled breast volume were also evaluated. SPECT images initially appear to yield observation of lesions smaller than those seen in scintimammography, with up to twice the SNR and contrast. Due to greater positioning flexibility of the system gantry, dedicated SPECT was able to both image a larger breast volume and view the chest wall where tumors may be missed in 2D imaging. Under this wide range of conditions, dedicated breast SPECT can detect and localize more lesions in a 3D volume.

Presented at the
Fourth International Workshop on the Molecular Radiology of Breast Cancer (MRBC)
Dresden, Germany
20-21 October, 2008

APPENDIX H: IEEE MRBC ABSTRACT

Novel Patient Acquisition Trajectories for Optimized Dedicated Breast SPECT Imaging

K. L. Perez[1,2], S. J. Cutler[2,3], P. Madhav[2,3], M. P. Tornai[1,2,3]
[1]*Medical Physics Program, Duke University, Durham, NC, USA*
[2]*Department of Radiology, Duke University, Durham, NC, USA*
[3]*Department of Biomedical Engineering, Duke University, Durham, NC, USA*

Acquisition trajectories for our dedicated breast SPECT camera can move contiguously but arbitrarily within a hemispherical volume, providing high resolution targeted data of a fully contoured patient's pendent breast. Created within a minute, these unique trajectories are personalized and optimized for each breast for a particular study. If a suspected lesion location is known prior to the scan, a trajectory can be created with many close and direct views of the lesion. Several scans were evaluated to validate this approach. A torso phantom with attached 1730mL breast containing a 2.1mL (0.8cm radius) spherical lesion was filled with clinical levels of radioactivity: heart:liver:torso:breast:lesion concentration ratio 3:12:1:1:10. Acquisition trajectories included: 1) vertical axis of rotation (VAOR) where the camera rotates around the breast, parallel to its central axis; 2) tilted parallel beam (TPB) where the camera rotates with a fixed polar tilt (15° or 45°) around the breast's central axis; 3) circle plus arc (CPA), where the camera arcs from 15° to 45° along the length of the breast and then rotates around the breast at a fixed 45° tilt; 4) projected sine wave (PROJSINE) where the camera traverses azimuthally about the breast while varying the polar tilt in three sinusoidal lobes from 15° to 45° peak-to-valley; and 5) saddle where the camera orbits the breast in two lobes from 15° to 45°. These trajectories were investigated to minimize the contamination from the heart, liver and torso and obtain the best breast lesion signal. PROJSINE trajectories can recover the breast's true, known shape as well as image into the chest wall. Altering the camera's azimuthal starting position reduces cardiac and hepatic contamination. However, more than one trajectory may provide equivalent image quality. Acquisition trajectories can be created to meet specific imaging goals which consider patient factors, such as breast size, lesion location and cardiac and hepatic uptake.

Presented at the
Fourth International Workshop on the Molecular Radiology of Breast Cancer (MRBC)
Dresden, Germany
20-21 October, 2008